# Primitive-Equation-Based Low-Order Models with Seasonal Cycle. II. Application to Complexity and Nonlinearity of Large-Scale Atmosphere Dynamics

Ulrich Achatz

Leibniz-Institut für Atmosphärenphysik an der Universität Rostock

Kühlungsborn, Germany

J.D. Opsteegh

KNMI, De Bilt, The Netherlands

submitted to *J. Atmos. Sci.* June 17, 2001

revised April 2, 2002

**Abstract**

A recently developed class of semi-empirical low-order models is utilized for the reexamination of several aspects of the complexity and nonlinearity of large-scale dynamics in a GCM. Given their low dimensionality, these models are quite realistic, due to the use of the primitive-equations, an efficient EOF basis and an empirical, seasonally-dependent, linear parameterization of the impact of unresolved scales and not explicitely described processes. Fairly different results are obtained with respect to the dependence of short-term predictability or climate simulations on the number of employed degrees of freedom. Models using 500 degrees of freedom are significantly better in short-term predictions than smaller counterparts. Meaningful predictions of the first 500 EOFs are possible for 4-5 days, while the mean anomaly correlation for the leading 30 EOFs stays above 0.6 for up to nine days. In a 30-EOF model this is only six days. A striking feature is found when it comes to simulations of the monthly mean states and transient fluxes: The 30-EOF model is performing just as well as the 500-EOF model. Since similar behaviour is also found in the reproduction of the number and shape of the three significant cluster centroids in the January data of the GCM, one can speculate on a characteristic dimension in the range of a few tens for the large-scale part of the climate attractor. A failure diagnosed in the predictability of climate change by our statistical-dynamical models indicates that the employed empirical parameterizations are actually climate-dependent. Before applying such models to climate change studies the major problem of predicting this dependence on the large-scale flow would first have to be solved. In a further analysis no support is found for the classic hypothesis that the observed cluster centroids, indicating multimodality in the climate statistics, can be interpreted as quasi-steady states of the GCM's low-frequency dynamics.

# 1 Introduction

In the light of the ever increasing complexity of the most realistic atmospheric general circulation models (GCM), low-order models have always been a helpful additional tool scientists have resorted to when the exploration of the fundamental dynamics was the aim. Earlier representatives (e.g. Lorenz, 1963; Charney and DeVore, 1979; Legras and Ghil, 1985; Vautard and Legras, 1988) have only been in qualitative agreement with observations. Although a lot could be learned from these simple models, the validation of proposed mechanisms was hampered by this limitation. Therefore, improving the realism of low-order models has long seemed desirable. This would not only provide a more solid basis for the lessons they can teach us but possibly also extend the corresponding curriculum to new fields of research. Consequently, later examples show an increasing degree of similarity with the actual atmosphere (e.g. Vautard, 1990; Selten, 1995, 1997a,b; Kwasniok, 1996, 1997; Hannachi, 1997; Achatz and Branstator, 1999, d'Andrea and Vautard, 2001). Nonetheless, a perfect small model, using a theoretical minimal number of degrees of freedom while completely reproducing daily weather and low-frequency climate, is still a distant aim, at most visible at the far horizon, if existing at all.

Recently some new progress has been made by introducing primitive-equation dynamics and seasonality into the field. In a companion paper (Achatz and Opsteegh, 2002, henceforth called AO) a method has been described for the development of corresponding semi-empirical models, combining a primitive-equation-based dynamical core for the nonlinear interactions with an empirical, seasonally-dependent, linear closure. This parameterizaton shall describe simultaneously all diabatic and viscid processes, as well as the impact of unresolved scales onto the resolved ones. The model variables are the expansion coefficients of the atmosphere with respect to a set of three-dimensional empirical

orthogonal fuctions (EOF). If compared to equally-dimensioned counterparts in Achatz and Branstator (1999, henceforth called AB), our models exhibit a much enhanced capability to correctly predict the tendencies of the same GCM that had provided the data set used for the determination of both EOFs and empirical closure (ECHAM3/LSG, Voss et al., 1998). This success motivated further tests and applications we want to report here.

We have first tested basic properties of our semi-empirical models, such as their ability to predict the daily weather in the GCM and simulate its climate, and their applicability to climate change studies. Simultaneously the predictability tests and climate simulations have provided valuable information with respect to the minimal number of degrees of freedom necessary for a correct dynamical description of the atmosphere. This fundamental theoretical problem is tightly linked to that of the dimension of the climate attractor. Quite a few attempts have been made at corresponding estimates by statistical methods (e.g. Fraedrich et al., 1995; Toth, 1995; Wang and Shen, 1999). However, the statistical approach may overlook degrees of freedom which, although small in contribution to the variance, might still be indispensable for a faithful simulation of a system. On the other hand it can also be that in spite of a rather large overall dimension small subsystems exist which are so loosely connected to the rest that a good self-consistent description of those subsystems is possible, incorporating the interaction with the remainder in parameterized form only. An example might be a subspace spanned by the large scales. Systematically reducing the dimension of our EOF models and examining their properties could possibly help in detecting such quasi-autonomous subsystems.

Another question we want to address concerns the origin of weather regimes and the associated multimodality of the atmospheric propability distribution. Charney and DeVore (1979) have put forward the now classic hypothesis, modified later in various

degrees, that multimodality reflects the existence of multiple equilibria of the flow equations. Motivated by the increase of detail in our models, while retaining simplicity, we have decided to reexamine this problem. For this we have first verified that the GCM exhibits multimodal behaviour, and that the reduced models are reproducing it. Next we have investigated whether or not the afore-mentioned hypothesis can explain the observed regime behaviour. Our results provide interesting additional constraints to be taken into account by any successful theory on the origin of weather regimes.

The article is structured as follows: Section 2 gives a very brief summary of the main characteristics of the reduced models we are using. In Section 3 we analyze their ability to simulate the GCM in its present climate state. We first discuss their capability to predict the daily weather in the GCM and to simulate its seasonally-dependent climate statistics. Next we examine the existence of multimodality in the GCM and the reduced models, and compare the corresponding regimes. In section 4 the difficult problem of climate change is addressed. Section 5 contains an extensive test of the multiple quasi-stationarity hypothesis for the origin of multimodality. Section 6 summarizes and discusses the results.

## 2 A brief model description

For better readability a very short description of our semi-empirical reduced models shall be given here. For any details the reader is referred to AO. The models are intended to describe the dynamics of a subsystem of the atmosphere part of the coupled atmosphere/ocean GCM ECHAM3/LSG (Voss et al., 1998). This subsystem consists of winds and (the square root of) potential temperature on the three levels at $\sigma = 0.167$, 0.500, and 0.833. $\sigma = p/p_s$ where $p$ and $p_s$ are pressure and surface pressure, respectively. The

horizontal discretization is given by a 64×32 Arakawa-C-grid (Arakawa and Lamb, 1981). External Kelvin waves are not taken into account so that the actual degrees of freedom for the wind field are the baroclinic parts of the horizontal flow field, and the streamfunction of the barotropic part. The number of grid-point variables describing this subsystem is $n = 16256$.

Denoting the $n-$dimensional state vector by $\mathbf{X}$, we use the expansion

$$\mathbf{X}(t) = \overline{\mathbf{X}} + \sum_{\nu=1}^{N} a_\nu(t)\mathbf{e}^\nu + \boldsymbol{\rho}(t) \tag{1}$$

into its long-time mean $\overline{\mathbf{X}}$ in the GCM data, $N \ll n$ leading EOFs $\mathbf{e}^\nu$, and a residual error $\boldsymbol{\rho}$ which is orthogonal to the EOFs. Let a scalar product $(\mathbf{X}, \mathbf{Y}) = \mathbf{X}^t\mathsf{M}\mathbf{Y}$ be defined by the metric $\mathsf{M}$. Then, projection of the discretized dry-adiabatic primitive-equation tendencies $\mathbf{g}(\mathbf{X})$ for our subsystem (the dynamical model core) onto the EOFs, and adding some time-dependent closure yields the reduced-model equations

$$\dot{\mathbf{a}} = \mathbf{t}(\mathbf{a}) + \mathbf{F}(t) + \mathsf{L}(t)\mathbf{a}\,. \tag{2}$$

Here $\mathbf{a}$ denotes the $N$-dimensional vector of expansion coefficients $a_\nu$, and $\mathbf{t}$ the corresponding tendency vector of the projected model, i.e.

$$t_\nu(\mathbf{a}) = (\mathbf{e}^\nu, \mathbf{g}(\overline{\mathbf{X}} + \sum_{\nu=1}^{N} a_\nu(t)\mathbf{e}^\nu))\,. \tag{3}$$

The metric we use is the total energy metric, i.e. ($\mathbf{X}$,$\mathbf{X}$) is the total energy conserved by the dynamical core. Together with the first- and second-moment statistics of the GCM it also defines the basic EOFs. The empirical closure, describing all diabatic and viscid processes, and parameterizing the impact of the unresolved scales, is given by

$$\mathbf{F}(t) = \mathbf{F}_0 + \sum_{n=1}^{2} [\mathbf{F}_n^c \cos(n\Omega t) + \mathbf{F}_n^s \sin(n\Omega t)] \tag{4}$$

$$\mathsf{L}(t) = \mathsf{L}_0 + \sum_{n=1}^{2} [\mathsf{L}_n^c \cos(n\Omega t) + \mathsf{L}_n^s \sin(n\Omega t)] \tag{5}$$

where $\Omega$ is the angular frequency of the earth's circumsolar orbit. Both EOFs and empirical closure have been extracted from GCM data.

The model integration uses a semi-implicit timestep in which the seasonally-independent linear dynamics (of the projected model and the empirical corrections) is treated implicitely, and the rest by an explicit leapfrog with time filter (Asselin, 1972).

# 3 Comparison between the EOF models and the GCM

As has been shown by AO, the above-described low-order semi-empirical models, with a dimension between 10 and 500 EOFs, predict the instantaneous tendencies of the GCM reasonably well. The corresponding relative tendency errors were markedly below those found for semi-empirical EOF models developed by AB with the help of a quasigeostrophic two-layer model core. We now discuss how this transmits into a similarity between GCM and reduced models with respect to meteorological standard features. First short-term predictions are investigated, then the first- and second-moment climate, and finally recurrent anomalies.

## 3.1 Short-term predictions of the GCM

A natural question to ask is how well our low-order models can approximate the local structure of the GCM's attractor. Faithful reproduction of the instantaneous tendencies in the GCM indicates that, if initialized on a GCM trajectory, the reduced models can follow it for quite some time. This has been quantified by calculating mean anomaly correlations

$$\text{m.a.c.}(\Delta t) \;=\; \frac{\sum_{i=1}^{I} \left(\mathbf{a}_{model} - \mathbf{a}^s, \mathbf{a}_{data} - \mathbf{a}^s\right)(t_i + \Delta t)}{\sum_{i=1}^{I} \left[\| \left(\mathbf{a}_{model} - \mathbf{a}^s\right)(t_i + \Delta t)\|^2 \| \left(\mathbf{a}_{data} - \mathbf{a}^s\right)(t_i + \Delta t)\|^2\right]^{1/2}} \qquad (6)$$

from integrations initialized twice-daily for all days of nine years of GCM data (i.e. $I = 6480$). The seasonally dependent mean state in the GCM data is denoted by $\mathbf{a}^s(t)$.

The results are shown in figure 1. The upper panel displays the decay of the mean anomaly correlation between trajectories of the 500-EOF model and GCM trajectories, calculated within the subspaces spanned by the leading 30, 200, or 500 EOFs. Obviously, the higher-dimensional subspaces, which encompass more small-scale features with shorter intrinsic time scales, are more difficult to predict. But even within these, predictions of the GCM with correlations exceeding 0.6 can be made for up to 4.5 days. Moreover, the first 30 EOFs can be predicted well for no less than nine days.

With respect to the dependence of the predictive skill on model resolution, AO had already shown that, the more patterns a reduced model was based on, the more accurately the instantaneous tendencies of the GCM were reproduced. Nonetheless, the performance at severe truncation was also not to be despised. So the relative tendency error of the 30-EOF model was not higher than 45.6%. This is also reproduced by the short-term integrations: Although, as will be seen below, the climate of the 30-EOF model is in very good agreement with that of the GCM, a comparison of the skill of the 30-, 200-, and 500-EOF model in predicting the leading 30 EOFs shows that the more complex models perform clearly better (lower panel of Fig. 1). This not withstanding, even the 30-EOF model can predict these degrees of freedom faithfully for up to six days.

## 3.2 Monthly-mean states and transient eddy fluxes

Next we move to leading characteristics of the global structure of the GCM's attractor, viz. the seasonally-dependent monthly-mean states and transient eddy fluxes. We first discuss the seasonal dependence of first and second moments in the 500-EOF model,

determined from 100-year integrations. As an example we have picked the monthly-mean zonal wind and meridional momentum flux by the transients (defined with respect to the monthly mean state) in the uppermost layer. The results agree with those observed for all other quantities. It appears that the meridional temperature transport simulated by the semi-empirical models is in better agreement with the GCM than the meridional momentum transport so that the latter provides a more critical test of the simulated second moments. Figures 2-5 show the January and July means of the zonal wind and the meridional momentum transport by that part of the transients projecting onto the leading 500 EOFs, for both the 500-EOF model and the GCM. The mean states of the GCM are very well reproduced by the reduced model. The momentum transport is simulated well, albeit with a somewhat too weak intensity. The overall seasonal dependence of the first- and second-moment statistics of the 500-EOF model is thus in quite good agreement with that of the GCM.

How does this comparison depend on the number of basic EOFs? AB have noted that their models are best reproducing the first and second moments of the GCM if the chosen resolution was not too fine. An optimum has been found in the range between 30 and 70 basis patterns. This optimum itself might be due to an inability of the quasigeostrophic two-layer model core, used there, to accurately deal with the smaller-scale features represented by the trailing EOFs. However, the interesting aspect of their result is that, as long as the number of basis patterns is larger than 30, the lower-order models are not performing worse than the higher-order ones in reproducing the large-scale aspects of the first- and second-moment structure of the climate attractor, thereby indicating the possible existence of a low-dimensional large-scale subspace connected to the rest so loosely that self-consistent modelling of it is possible to a high degree. The question arises whether we

can confirm this finding. In contrast to the models developed by AB ours have a seasonal cycle and employ as dynamical core the primitive equations. We have investigated to what extent this increase in incorporated details has an effect on the resolution-dependence of climate simulations, not only with respect to its very existence but also regarding the size of the above mentioned subspace. For example, it could have been conceivable that a seasonal cycle requires more than just 30 patterns for a well-performing model.

In agreement with the results of AB we find that lower-resolution models are simulating the first- and second-moment statistics of the GCM as well as the 500-EOF model. As objective measures for the comparison between EOF-model and GCM data we have used the seasonally-dependent relative error for the monthly-mean first moments,

$$\epsilon_1^m = \frac{\sum_{\nu=1}^{N} \left(\overline{a_\nu}^m_{model} - \overline{a_\nu}^m_{data}\right)^2}{\sum_{\nu=1}^{N} \left(\overline{a_\nu}^m_{data}\right)^2} , \tag{7}$$

and the corresponding second-moment error

$$\epsilon_2^m = \frac{\sum_{\nu=1}^{N} \sum_{\mu=\nu}^{N} \left(\overline{a'_\nu a'_\mu}^m_{model} - \overline{a'_\nu a'_\mu}^m_{data}\right)^2}{\sum_{\nu=1}^{N} \sum_{\mu=\nu}^{N} \left(\overline{a'_\nu a'_\mu}^m_{data}\right)^2} . \tag{8}$$

The upper index $m$, running from 1 to 12, indicates the month for which the time-mean (denoted by an overbar) has been calculated. $a'_\nu(t) = a_\nu(t) - \overline{a_\nu}^m$ denotes transients. Fig. 6 shows, for all models we have extracted from the data, the dependence of these errors on the number of basic EOFs, both for January and July. Once again there seems to be an optimum at a dimension of 30. Figures 7 and 8 show the corresponding comparison between the transient meridional momentum transport in the uppermost layer in the GCM and in the 30-EOF model. In January the 30-EOF model is clearly in better agreement with the GCM than the 500-EOF model. More insight is offered by Figure 9. There we show the relative climate error

$$\epsilon_c = \frac{1}{24} \sum_{m=1}^{12} \left(\epsilon_1^m + \epsilon_2^m\right) , \tag{9}$$

calculated within different subspaces. In contrast to AB, we find that within the subspace of the leading 10 or 30 EOFs the 30-EOF model is doing as well as the 500-EOF model, but not better. Obviously, the superiority of the 30-EOF model over the 500-EOF model as displayed in figure 6 results from a somewhat worse performance of the 500-EOF model in simulating patterns 31 to 500. However, once again there is a clear local optimum at a model resolution of 30 EOFs. We conclude that the major result of AB is also found for the present semi-empirical primitive equation models with seasonal cycle.

### 3.3 Recurrent anomalies

Let us now turn to nonlinear signatures in the climate statistics. Clearly, the climate system is nonlinear. It may however be asked to what detail its nonlinearity is relevant for understanding available observations. To some degree it might be sufficient to view nonlinear dynamics as providing some completely irregular forcing and an effective damping. Assuming maximum irregularity of the forcing in the time domain, i.e. stochastic white noise, linear models have been shown to reproduce a wealth of features of the observed climate system, be it atmospheric transient-eddy activity (e.g. Farrell and Ioannou, 1993, 1994; Whitaker and Sardeshmukh, 1998; DelSole and Hou, 1999; Zhang and Held, 1999) or tropical SST variability (Penland and Matrosova, 1994; Penland and Sardeshmukh, 1995). The picture arising is intriguingly simple but nonetheless might also have its limitations. As is well known (e.g. Honerkamp, 1994) the probability density function (PDF) of a stochastically forced linear system is a Gaussian. If the PDF is known to have this form, then it can be completely defined by first- and second-moment statistics as described above. However, should any deviations from Gaussian statistics be detected, these would indicate the necessity of a more complex model for the active nonlinearity than additive

white noise. Multiplicative noise could be a possibility, as well as explicit deterministic nonlinear dynamics.

Although they are still a matter of debate, indications for persistent and recurrent anomalies, which might also have relevance for the predictability of the low-frequency part of atmospheric variability, have been found by several authors (e.g. Hansen and Sutera, 1986; Dole, 1986; Molteni et al., 1988, 1990, Mo and Ghil, 1988; Michelangeli et al., 1995). These could imply the existence of more than one local maximum of the atmospheric PDF, i.e. they are intrinsically associated with its non-Gaussian character. Understanding their origin has been a favorite application of low-order models over the years. We have therefore examined whether the GCM we have used for our work exhibits such features, and, finding this to be true, whether the semi-empirical models reproduce them.

For this we have resorted to cluster analysis. The existence of more than one significant cluster in a data set indicates asymmetries in the corresponding PDF which might be related to multimodal behavior. We have basically used the method described in Michelangeli et al. (1995), with the modification that, instead of pattern correlations, we have chosen absolute distances between anomalous states as a measure of similarity. Furthermore, we have considered global anomalies involving all prognostic variables.

To be more precise, given a data set of state vectors $\mathbf{b}$, and a predefined number $K$ of centroids $\mathbf{b_k}$ $(k = 1, 2, \ldots, K)$, each state is associated with the closest centroid, i.e. it is said to belong to the corresponding cluster $M_k$. The dynamic cluster method (Diday and Simon, 1976) determines the centroids such that the sum of variances within the clusters is minimized, i.e.

$$\sum_{k=1}^{K} \sum_{\mathbf{b} \in M_k} \|\mathbf{b} - \mathbf{b_k}\|^2 \tag{10}$$

must be as small as possible. The calculation is done using a simple nonlinear optimization algorithm: Starting with some initial guess for the centroids the available states are ordered in clusters, followed by an update of the centroids by taking the mean of each cluster. This procedure is repeated until convergence of the centroids is observed.

Obviously, this analysis alone does not yet provide useful information. One will always find a set of cluster centroids minimizing (10). The question is whether they are significant in the sense that they are indicating a clear deviation of the PDF from a Gaussian form. Here helps the observation that in the case of a unimodal distribution which is rotation-invariant with respect to any axis through its maximum an infinite set of solutions to the minimization problem exists. Furthermore, should the data be not quite completely sampled, local minima in the cost function (10) are bound to occur to which the algorithm may converge. Different initial guesses for the centroids will only result in one final optimal solution if the PDF has a relatively marked multimodal structure. Therefore, choosing a random set of initial guesses, performing the cluster analysis, and finally checking whether the obtained centroids are identical or not, provides a possibility to check the significance of the cluster partitions. As a measure of the uniqueness of the partition in a given number of clusters, i.e. the classifiability of the data set, we have used an index which is defined in the following way: Let $P$ and $Q$ be two partitions of the data set in $K$ clusters with corresponding cluster centroids $\mathbf{b_k^P}$ and $\mathbf{b_k^Q}$. The difference $d(P,Q)$ between the partitions is given by

$$d(P,Q) \;=\; \max_{1\le i\le K}\min_{1\le j\le K} \|\mathbf{b_i^P}-\mathbf{b_j^Q}\|^2. \tag{11}$$

It only vanishes when the two partitions are identical. Given a set $S_P$ of $M$ partitions obtained from random initial guesses our classifiability index $C$ is defined via

$$C^{-1} \;=\; \frac{1}{M(M+1)}\sum_{P\in S_P}\sum_{Q\in S_P\setminus\{P\}} d(P,Q). \tag{12}$$

The data set is only then said to be classifiable into $K$ clusters if the classifiability index is significantly larger than the corresponding indices obtained from cluster analyses of random data sets with Gaussian PDF having the same first and second moments.

In our case we have taken as raw data the coefficients belonging to the $N$ leading GCM-EOFs from a specific month, either from the GCM integration or from one of the semi-empirical models. Then nonoverlapping $n$-day averages have been formed. These low-pass filtered states have been analyzed for (low-frequency) EOFs, of which the leading $\tilde{N}$ have been picked. The corresponding low-frequency-EOF expansion coefficients of the anomalies with respect to the long-time monthly mean form the state vector $\mathbf{b}$. As in Michelangeli et al. (1995) the number of initial guesses for the centroids was $M = 50$. They have been obtained from a random vector generator producing a Gaussian statistics with the same first and second moments as the analyzed data. For comparison 100 random data sets of the same length and with that same Gaussian statistics have been generated which have then also been analyzed for clusters. The obtained classifiability indices have been ordered with respect to their magnitude and the 10th and 90th of them have then been picked so as to provide an estimate of the confidence limits for classifiability indices obtainable from data with unimodal Gaussian PDF.

In a first attempt we have analyzed 1500 January or July months from the GCM. The leading $N = 30$ EOFs have been picked. 5-day averages have been taken, and no further data compression has been performed, i.e. $\tilde{N} = 30$. The resulting classifiability inidices are shown in figure 10. They indicate that the July PDF can essentially be described by a unimodal Gaussian distribution. However, this is not the case for January. There is a significant classifiability into three clusters. Additionally, we have checked whether we have taken enough data for the analysis, by doing a second examination of January

months from the first 700 years. The result was positive: Not only was the same behavior of the classifiability index identified, but a comparison of the centroids themselves also showed that they are virtually the same if determined from 700 or 1500 years.

Henceforth we have therefore focussed our attention on the January PDF, and investigated whether the reduced models can simulate this behaviour. The analysis of 1500 January months has been redone with data from the 30-, 200-, and 500-EOF model. Figure 11 contains the classifiability indices determined for the 30-EOF model data. In addition to a weak signal at five clusters, the same significant classifiability into three clusters is discernible. Furthermore, the mean centroids identified for this partition are very similar to the ones obtained from the GCM data. This is displayed in Figures 12-14 where the anomalies of the centroids with respect to the mean January state in the barotropic stream functions for both reference partitions (GCM and semi-empirical model) are shown. These reference partitions are defined as those among the $M$ determined three-cluster partitions which have on average the smallest distance to the other ones. Additional experiments have been done in which the filtering period has been varied between 5 and 30 days, and the compressed dimension $\tilde{N}$ was also changed from 30 to 20, 10, or 5. The results are always about the same. Reproducibility has also been checked by analyzing 3000 instead of 1500 years, with no different outcome.

The relation between clusters and EOFs in the respective models shows reasonable similarities as well, but also highlights differences. In an attempt to get some insight into whether and how the leading low-frequency EOFs can be understood on the basis of the clusters, we have calculated, for 5-d low-pass filtered January data (1500 years projected onto the leading 30 GCM EOFs) from both the GCM and the 30-EOF model, the pattern correlations, between the anomalies of the three clusters with respect to the

monthly-mean state, and the 30 low-frequency EOFs which have been used in the cluster algorithm. As was to be expected, there is virtually no correlation with the trailing EOFs so that Figure 15 only displays those for the leading 10 patterns. As for similarities, both models show cluster 1 to project basically on EOF 1. Cluster 3 has a strong negative projection onto the same pattern, but also a considerable positive correlation with EOF 2. Cluster 2 is mostly negatively correlated with EOF 2. So it appears that, roughly speaking, the two leading EOFs can be interpreted as signals of the differences between clusters 1 and 3 (EOF 1) and clusters 2 and 3 (EOF 2). Both models agree in essentially the two leading EOFs spanning the three cluster anomalies. Differences are, however, not to be overlooked either: In the reduced model the clusters are spread a bit more over the trailing EOFs. Furthermore, the GCM cluster 2 shows a nonnegligible contribution of EOF 1, in contrast to its counterpart from the reduced model. However, these and other discrepancies notwithstanding, the agreement in the recurrent-anomaly statistics of GCM and 30-EOF model is quite striking.

Cluster analyses of the 200- and 500-EOF model have also been done, in order to analyze the dependence of our results on the truncation. These revealed that again the separation into three clusters is significant, and that the first two GCM clusters are reproduced (among these cluster 1 especially well). Cluster 3 seems to be more difficult to reproduce since none of the larger models yields a third cluster resembling it.

Summarizing the last three subsections, we conclude that lower-dimensional reduced models using as few as 30 degrees of freedom simulate the climate statistics of the GCM quite well, whereas the larger semi-empirical models have a special advantage at reproducing its short-time behavior.

# 4 Response to external perturbations

As pleased as as one might be about the ability of our models in simulating the GCM's climate, the important question remains whether they can also be used for studies of climate change or climate variability on ultra-long time scales. Actually, this poses an enormous challenge since it necessitates realistic response of the model to external influences (of the lower surface or radiation) and, more specifically, to changes in them. Problems are to be expected since both optimal patterns and the empirical parameterizations are conditioned on the climate of the data set from which they have been extracted. For a study of this problem we have done some experiments with the GCM in which an anomalous heat source has been placed over the equator. Its form is the same as used by Branstator and Haupt (1998): It has a circular shape (radius 1500 km) with the strength increasing linearly from zero at the outer edge to a maximum value of 2.5 K/d at the center. The vertical shape is sinusoidal, with the two nodes being at the model's top and bottom surface, and the single maximum at $\sigma = 0.5$. As a reference the GCM has first been integrated under perpetual-january conditions (without coupling to the ocean) and an anomalous response has been determined by subtracting the resulting mean states from the corresponding means from an integration without anomalous heating. The experiment was repeated with the semi-empirical 500-EOF model. The result desired was that the two experiments yield the same response.

In a first attempt the reduced model did not respond to the anomalous heating. Inspection showed this to be a consequence of the weak variability of tropical temperature. Corresponding anomalies are rather represented by the trailing EOFs so that anomalous tropical heat sources do not project well onto the leading patterns. We have therefore repeated the original EOF analysis (as described in AO), this time however splitting the

total state space into two subspaces, one subspace comprising the thermodynamic variable $\tau$ (the square root of potential temperature) in the latitude band from 11.25°S to 11.25°N, i.e. at the equator and at the two grid-latitudes north and south of it, and the other subspace comprising the remaining prognostic variables. It is easily checked that these two subspaces are orthogonal so that an EOF analysis within them yields two sets of basis patterns with the same property. The analysis of how many tropical-$\tau$ EOFs are needed to explain the variance orthogonal to the two leading patterns, which essentially capture the seasonal cycle, showed that 200 must be used for getting above the 90%-limit. In the other subspace the corresponding number is 500. It has then been examined how well the anomalous heating projects onto the overall $700 = 200 + 500$ EOFs. The result was encouraging: Among the 24 heat sources we have examined (longitude at 0°E, 15°E, ..., 15°W) none was found which projects onto the new basis to less than 80%. We have therefore determined, in the same manner as described in AO, a semi-empirical 700-EOF model from 1510 years of data which was then tested for its reponse to the anomalous heating.

Three cases have been studied with anomalous heating at 120°E, 150°E, and 180°E. The GCM has been integrated over 36 months, of which the last 30 months have been used for the analysis. The resulting signal-to-noise ratio was sufficient for our needs. The reduced model has been integrated over 5500 days. Here the last 5000 days have been analyzed. The comparison between the two responses was only partially satisfying: Whereas there is some similarity in the reponses to heating at 150°E (Fig. 16) and 180°E, the reduced model does not reproduce the GCM's response to anomalous heating at 120°E. It was checked whether this is due to an inability of the chosen EOFs to represent the response, but this is not the case.

In further experiments the heat source has been placed at 30°N so as to exclude the possibility that problems arise from wave-train reflection at the subtropical zero-wind line which might be placed differently in the GCM and the reduced model. However, also in these experiments the reponse of the GCM and the reduced model did not agree well with each other.

So we must conclude that there are important feedbacks between anomalous external forcing and anomalies in the parameterized processes (e.g. latent heat release) which are not captured by our static parameterizations. Rather one would have to know how they depend on the external forcing in order to be able to predict the atmosphere's behaviour from the reduced model.

# 5 Recurrent anomalies and quasi-stationarity

Even without the possibility, at the present state of development, to use reduced models for climate-change studies, the option remains to apply them in investigations on the mechanisms responsible for the climate as it is. As an example, low-order models have frequently been applied in studies on multimodality in the atmosphere. The semi-empirical models presented here exhibit an enhanced degree of completeness in the incorporated features. They are global, use the primitive equations, they are optimized so as to predict the local tendencies observed in a GCM, and they have been shown to produce a realistic climate. The latter, including the simulated multimodality, holds for a model using no more than 30 degrees of freedom, so that it seems worthwhile to reexamine its nonlinear dynamics for a deeper understanding of the identified recurrent anomalies.

Actually, we do not attempt to give a complete analysis of the dynamics of the 30-EOF model, but we will focus on the question how well the clusters can be explained (in the

best of all cases even be predicted) as stationary states of the model. This hypothesis goes back to Charney and DeVore (1979) and has later on, with modifications, been taken up by several authors (e.g. Legras and Ghil, 1985; Vautard and Legras, 1988; Michelangeli et al., 1995; Hannachi, 1997). It has been recognized that stationarity is more likely to play a role for the low-frequency part of the dynamics, in the sense that it is only encountered in some time-mean way, with the transients providing possibly important feedbacks.

In an investigation of corresponding frequency spectra (not shown) it was found that the leading 30 EOFs are dominated by longer time scales. It could therefore not a priori be excluded that the semi-empirical model treats the impact of short time scales already in an approriately parameterized mean way. In a first attempt we have therefore searched for steady states of the semi-empirical model itself. This has been done by searching for stationary states $\mathbf{a_s}$ minimizing the squared relative model tendency $\|\dot{\mathbf{a}}(\mathbf{a_s})\|^2/\overline{\dot{\mathbf{a}}^2}$ so that it is below a certain threshold (the time of the year was held fixed at January 15th). For this we have used a nonlinear optimization routine which needs as input a first guess. As such we have tried all 9000 January 5-day means which had been used for the cluster analysis. Only solutions with squared relative tendency less than $1.0 \cdot 10^{-6}$ have been accepted so that they all represent states which are stationary over periods at least 1000 times longer than the typical time scales produced by the model (a few days). Varying this criterion does not change the outcome greatly. We have identified 22 steady states. Comparison of these with the three cluster centroids did, however, not yield a single pair with convincing similarity. The same holds for the three local tendency minima we have found after initializing the search with the cluster centroids themselves. One general feature is that the identified states all exhibit much stronger anomalies with respect to the January mean state than the cluster centroids.

Since the cluster partition has been determined from 5-day means, a reason for this discrepancy could have been that the model is not filtered in this way, so that the mean impact of transients, shown by others to be potentially important, is not taken into account as an additional force on the time-filtered state. Thus we have formulated a low-frequency reduced model which describes this additional forcing in the best possible way. The degrees of freedom of this model are summarized in the $\tilde{N}$-dimensional vector $\mathbf{b}$ , as described in section 3.3, of expansion coefficients of the time-filtered data with respect to their (low-frequency) EOFs. The dynamical equations of the low-frequency model have been obtained by the same procedure as used in the determination of our semi-empirical models from the GCM data: We have projected the equations of the 30-EOF model onto the low-frequency patterns (i.e. projected the primitive equations onto the patterns) and fitted a constant forcing term and a linear term (without slow seasonal dependence) such that the relative squared tendency error between data (tendencies from 5-day averages of exact tendencies from the 30-EOF model) and low-frequency model is as small as possible. The model equations are thus

$$\dot{b_\nu} \;=\; F_\nu^p + \sum_{\mu=1}^{\tilde{N}} L_{\nu\mu}^p b_\mu + \sum_{\mu=1}^{\tilde{N}} \sum_{\rho=1}^{\tilde{N}} N_{\nu\mu\rho} b_\mu b_\rho + F_\nu^c + \sum_{\mu=1}^{\tilde{N}} L_{\nu\mu}^c b_\mu. \qquad (13)$$

$\mathbf{F^p}$, $\mathsf{L^p}$, and $\mathsf{N}$ are determined by the projection, whereas $\mathbf{F^c}$ and $\mathsf{L^c}$ are the closure terms which minimize the relative tendency error. We want to mention that our closure approach is more comprehensive than the one taken by Hannachi (1997) who has parameterized unresolved scales and processes by a constant forcing.

In order to get some overview, the filtering period in days, $n$, and the model dimension $\tilde{N}$ have been varied. Low model dimensions are motivated by the observation that, in the case of 5-day-filtered data, the leading five low-frequency EOFs explain 98% of the cluster centroid anomalies with respect to the January mean. 95% are already explained

by the leading three EOFs. This justifies, in hindsight, the approach by Hannachi (1997) who showed that a projection of a quasigeostrophic two-layer model onto only two EOFs, supplemented by a simple empirical closure, can yield interesting steady states which have a structure similar to the recurrent anomalies that he has identified in a GCM data-set (integrated under perpetual January conditions). There seems to be a strong projection of the recurrent anomalies onto the leading EOFs. That this is remarkable follows from the fact that in our time-filtered 30-EOF-model data no fewer than 20 low-frequency EOFs are needed for explaining 90% of the total variance.

The various low-frequency models having been analyzed for steady states, squared relative distances have been calculated in the model state space between cluster centroid anomalies and steady state anomalies, normalized by the squared norm of the cluster centroid anomalies. For each centroid the closest steady state has been identified. In the case that the same steady state was closest to several centroids, it was associated with the one it is closest to, and among the remaining steady states a new search for steady states closests to the other centroids was done. The results are summarized in table 1. The sobering conclusions one can draw from it is that in no case satisfying closeness between steady state and cluster centroid could be found. There seems to be an advantage in the comparison of steady states of the five-dimensional models with the centroids which might be due to the strong projection of the latter onto the leading five low-frequency EOFs. On the other hand, the results for 3-dimensional models are already worse again so that there is also a lower limit in the dimension appropriate for the analysis, which is higher than the one used by Hannachi (1997). Figure 17 shows the two steady states in the 5-dimensional 5-day-low-pass model which are closest to centroids 1 and 3. The strong similarities in the patterns of steady state 3 and centroid 3 (pattern correlation is

0.97) and steady state 1 and centroid 2 (pattern correlation 0.77) are striking but, as in the steady state analysis of the original 30-EOF semi-empirical model, the steady state anomalies are much stronger than those of the corresponding cluster centroids.

# 6 Summary and Discussion

Given the many interesting lessons low-order models have already taught us on basic mechanisms in atmosphere dynamics, continuous improvement of their realism, and thereby also their applicability to various outstanding problems, seems to be a worthwhile undertaking. Contributing to this effort we have investigated the properties of a newly developed class of semi-empirical reduced models (Achatz and Opsteegh, 2002). These are based on global three-dimensional EOFs, each of them encompassing a whole atmospheric state. Primitive-equation dynamics is used for the description of the nonlinear interactions between the basis patterns, while the impact of viscid and diabatic processes, as well as that of the unresolved scales, is captured by an empirical linear parameterization. The EOFs and the empirical parameterization have been extracted from the data of a long GCM integration. Both the GCM and the reduced models include the seasonal cycle.

In addition to an investigation of the skill of the semi-empirical models at predicting and simulating the GCM we have addressed two questions with regard to atmospheric dynamics. First, we were interested how the comparison of the model behavior with that of the GCM depends on the number of basis patterns. It was hoped that this would yield new insights into the complexity of the climate attractor of the GCM, and thereby also, by analogy, of the atmosphere itself. Secondly, given the more comprehensive nature of our low-order models in comparison to previously published examples, we have revisited

the problem of multimodality, and reexamined its explanation based on multiple steady states.

First focussing on the local structure of the GCM attractor, mean anomaly correlations have been calculated between GCM trajectories and those of the various reduced models. Analyzing the 500-EOF model we have found that the GCM trajectories can be predicted with meaningful skill for up to 4.5 days in the state space spanned by all basis patterns. The leading 30 patterns are predicted well for up to nine days. An investigation of the effect of the model dimension reveals a decline of the short-term predictive properties with a decreasing number of basis patterns. Nonetheless, even a 30-EOF model can predict its degrees of freedom well for up to six days.

With regard to simulations of the first- and second-moment climate statistics we find, in agreement with the results of Achatz and Branstator (1999, in short AB) that a 500-EOF model is simulating the atmosphere's climate (as captured by the GCM) well, now however also in its seasonal dependence. This indicates that the seasonal cycle is re-arranging the respective role of the various atmospheric degrees of freedom rather than using different ones in different seasons. We have also reproduced the observation of the above mentioned authors that both first and second moments in the respective model state spaces are simulated just as well by lower-resolution models. The model based on only 30 patterns simulates the seasonally dependent mean states and transient fluxes based on its explicit degrees of freedom faithfully in a self-consistent manner.

A further feature we have looked at is non-gaussian statistics. Recurrent anomalies in GCM and reduced-model have been searched for by way of a cluster analysis. Care has been taken to detect statistically significant deviations in the PDF from purely Gaussian behavior. Measuring clustering in terms of real distances in phase space (using a total

energy metric) instead of pattern correlations (which is a weaker indication of similarity between states) we find in the GCM a significant partitioning into three clusters in January. The corresponding anomalies with respect to the climatological January state are not as prominent as expected in real nature (e.g. Michelangeli et al., 1995). Nonetheless a corresponding analysis of data from the reduced models shows that in all cases the same significant partitioning was reproduced. It is found that the 30-EOF model is performing especially well. It reproduces all three recurrent anomalies faithfully as well as the number of states found in their domain.

A caveat must be added concerning the present applicability of semi-empirical reduced models in the context of climate prediction. What might make them interesting for modelling past or future climate is their realism in combination with high integration speed. The 500-EOF model can be integrated over 100 years in about 4 hours, the 30-EOF model in three minutes (both on an NEC SX4). A conclusion one can draw from our work is that an essential part of the impact of the unresolved scales and physical processes can be described by linear parameterizations. However, the corresponding parameters had to be determined empirically from the GCM data. These are conditioned on the examined climate so that changes in external influences (from radiation, ocean, ice, soil etc.) should have an effect on them. For the present we have not undertaken an effort to predict as much of this climate-dependence as possible by using explicit physics parameterizations in the dynamical core wherever conceivable, or by trying advanced theoretical approaches such as renormalization group theory (Moise and Temam, 2000). This would have reduced the role of the empirical terms to handling only the most intricate feedbacks of the unresolved scales and physics onto the resolved scales which we are presently not able to predict on theoretical grounds. Not too surprisingly, we have therefore not been able to

use the semi-empirical reduced models for predicting the GCM's response to anomalous tropical heating. There is still plenty of room for improvements of reduced models, possibly eliminating this problem. Even at the present stage, however, it should be stressed that the problems with regard to climate change do not argue for the use of more basis patterns. Even though a more compact basis might be possible using more dynamically-oriented patterns such as principal interaction patterns (Hasselmann, 1988) or stochastic optimals (Farrell and Ioannou, 2001), at the examined truncation both the anomalous forcing and the true anomalous response are well represented by the chosen EOFs. Our findings rather point to the necessity of a climate-dependent parameterization scheme.

This deficit nothwithstanding, it remains a striking observation that a model using no more than 30 basis patterns can simulate many aspects of the GCM's climate as well as its higher-dimensional brothers. It is tempting to ask for explanations of this behavior. A detailed investigation is beyond the scope of our paper. However, it is interesting to observe that, although we confirm the result of AB in so far as lower-dimensional models are not doing worse in climate simulations than the larger ones, their superiority over the latter, if there is one at all, is not as marked any more. This might be due to the more realistic dynamical model core based on the primitive equations. Still the 500-EOF model has a somewhat reduced skill at dealing with the trailing EOFs, viz. the relative deviation between its first and second moments and the ones from the GCM is larger if calculated in the 500-EOF subspace, but this does not affect as strongly its ability to simulate the first- and second-moment statistics in the subspace of the leading 30 patterns as was the case in AB. It must be expected that further improvements in the dynamical model core, e.g. increased vertical resolution or explicit treatment of nonlinear physical processes, will finally lead to reduced models which get better as the number of basis patterns is

increased. After all, the GCM itself, projected onto the complete EOF basis, would be an EOF model yielding exactly the climate of the GCM data we are comparing the reduced models with.

Nonetheless, there are local optima in model resolution which may still survive further model developments. It might be speculated that the optimum of about 30 EOFs indicates the existence of a typical number characterizing the complexity of that large-scale part of the GCM's dynamics which can be simulated especially well in a self-consistent manner. Incorporation of only a few additional basis patterns could lead to a worsening of the model performance since they span dynamic components of smaller scale and higher frequency which can only be well described if all corresponding basis patterns are taken into account. Support for the notion that the local optimum we find at a few tens of basis patterns could be dynamically meaningful comes from previous attempts which have been undertaken at measuring the complexity of the large-scale part of the climate attractor in the form of a number of spatial degrees of freedom (dof). This has been done by comparing the distribution of squared distances, either between states or to the climate mean, to the distribution of a $\chi^2$-variable with a given number of degrees of freedom (Lorenz, 1969; Fraedrich et al., 1995; Toth, 1995), by using statistical field significance (Livezey and Chen, 1983; Wang and Shen, 1999), or by examining the variance of the correlation coefficient between states (Horel, 1985; Van den Dool and Chervin, 1986). All estimates found the dof of the atmosphere or GCMs to be in the range of between several tens and slightly above 100. This roughly agrees with the critical number we have found where it should be stressed that it is more the optimum at a few tens than the very number 30 we consider important. Further work is necessary to investigate the correctness of this picture but we think it could be a useful working hypothesis.

Since the 30-EOF model is reproducing the clusters of the GCM so well we have also looked at the question whether the thereby indicated multimodality of the GCM's PDF can be understood by relating the cluster centroids to the steady states of the model. For this both the reduced model itself has been analyzed and corresponding low-frequency versions. The latter project its dynamics further onto leading low-frequency EOFs, obtained by an analysis of low-pass filtered data from the 30-EOF model, and utilize in addition an empirically determined parameterization of the impact of transients. The lower dimension of these models (as also used by Hannachi, 1997) can be justified by the observation that the cluster centroids project much stronger onto the leading low-frequency patterns than the total variance. The results were not encouraging: None of the models we have looked at, i.e. also the 30-EOF model itself, have steady states which are convincingly similar to the cluster centroids. In a five-dimensional low-frequency model high pattern correlations between centroid anomaly and steady state anomaly could be found in two cases. However, even there a large difference in the amplitude of the anomalies was encountered. This is in agreement with the results of others (Michelangeli et al., 1995; Hannachi, 1997) so that one might question the usefulness of the concept of quasi-stationarity for the interpretation of PDF deviations from unimodal Gaussian behavior. Perhaps there is more perspective in the view of Itoh and Kimoto (1999) that ruins of multiple attractors, to be found at nearby values of some model parameters lead to the observed multimodal behavior. Anyway, interesting work is ahead of us, and hopefully reduced models will be able to contribute.

**Acknowledgements**

The authors are indebted to R. Haarsma, F. Kwasniok, G. Schmitz, F. Selten, and A. Timmermann for numerous discussions helping us in different phases of the work. Fur-

thermore we would like to acknowledge the helpful comments of C. Penland and two anonymous reviewers which have lead to substantial improvements in the manuscript. Special thanks are due to R. Voss for allowing us to use his GCM data. The enormous help of X. Wang in retreiving those data from the archives is also gratefully acknowledged.

# References


Achatz, U., and G. Branstator, 1999: A two-layer model with empirical linear corrections and reduced order for studies of internal climate variability. *J. Atmos. Sci.*, **56**, 3140-3160

Achatz, U., and J.D. Opsteegh, 2002: Primitive-equation-based low-order models with seasonal cycle. I. Model construction. *J. Atmos. Sci.*, subm.

Arakawa, A., and V. R. Lamb, 1981: A potential enstrophy and energy conserving scheme for the shallow water equations. *Mon. Wea. Rev.*, **109**, 18-36

Asselin, R., 1972: Frequency filter for time integrations. *Mon. Wea. Rev.*, **100**, 487-490

Branstator, G., and S.E. Haupt, 1998: An empirical model of barotropic atmospheric dynamics and its response to tropical forcing. *J. Climate*, **11**, 2645-2667

Charney, J., and J.G. DeVore, 1979: Multiple flow equilibria in the atmosphere and blocking. *J. Atmos. Sci.*, **36**, 1205-1216

d'Andrea, F., and R. Vautard, 2001: Extratropical low-frequency variability as a low-dimensional problem. I: A simplified model. *Quart. J. Roy. Meteor. Soc.*, **127**, 1357-1374

DelSole, T., and A.Y. Hou, 1999: Empirical stochastic models for the dominant climate statistics of a general circulation model. *J. Atmos. Sci.*, **56**, 3436-3456

Diday, E., and J.C. Simon, 1976: Clustering analysis. *Communication and Cybernetics 10 Digital Pattern Recognition*, K.S. Fu, Ed., Springer-Verlag, 47-94

Dole, R.M., 1986: Persistent anomalies of the extratropical Northern Hemisphere wintertime circulation: Structure. *Mon. Wea. Rev.*, **114**, 178-207

Farrell, B.F., and P.J. Ioannou, 1993: Stochastic dynamics of baroclinic waves. *J. Atmos. Sci.*, **50**, 4044-4057

Farrell, B.F., and P.J. Ioannou, 1994: A theory for the statistical equilibrium energy spectrum and heat flux produced by transient baroclinic waves. *J. Atmos. Sci.*, **51**, 2685-2698

Farrell, B.F., and P.J. Ioannou, 2001: Accurate low-dimensional approximation of the linear dynamics of fluid flow. *J. Atmos. Sci.*, **58**, 2771-2789

Fraedrich, K., C. Ziehmann, and F. Sielmann, 1995: Estimates of Spatial Degrees of Freedom. *J. Climate*, **8**, 361-369

Hannachi, A., 1997: Low-frequency variability in a GCM: Three-dimensional flow regimes and their dynamics. *J. Climate* , **10**, 1357-1379

Hansen, A.R., and A. Sutera, 1986: On the probability density distribution of planetary-scale atmospheric wave amplitude. *J. Atmos. Sci*, **43**, 3250-3265

Hasselmann, K., 1988: PIPs and POPs: The reduction of complex dynamical systems using principal interaction and oscillation patterns. *J. Geophys. Res.*, **93**, 11015-11021

Honerkamp, J., 1994: *Stochastic dynamical systems.* VCH Publishers, New York, USA

Horel, J.D., 1985: Persistence of the 500 mb height field during Northern Hemisphere winter. *Mon. Wea. Rev.*, **113**, 2030-2042.

Itoh, H., and M. Kimoto, 1999: Weather regimes, low-frequency oscillations, and principal patterns of variability: A perspective of extratropical low-frequency variability. *J. Atmos. Sci.*, **56**, 2684-2705

Kwasniok, F., 1996: The reduction of complex dynamical systems using principal interaction patterns. *Physica D*, **92**, 28-60

Kwasniok, F., 1997: Optimal Galerkin approximations of partial differential equations using principal interaction patterns. *Phys. Rev. E*, **55**, 5365-5375

Legras, B., and M. Ghil, 1985: Persistent anomalies, blocking and variations in atmospheric predictability. *J. Atmos. Sci.*, **42**, 433-471

Livezey, R.E., and W.Y. Chen, 1983: Statistical field significance and its determination by Monte Carlo techniques. *Mon. Wea. Rev.*, **111**, 46-59

Lorenz, E.N., 1963: Deterministic nonperiodic flow. *J. Atmos. Sci.*, **20**, 130-141

Lorenz, E.N., 1969: Atmospheric predictability as revealed by naturally occurring analogues. *J. Atmos. Sci.*, **26**, 636-646

Michelangeli, P.-A., R. Vautard, and B. Legras, 1995: Weather regimes: Recurrence and quasi stationarity. *J. Atmos. Sci.*, **52**, 1237-1256

Mo, K.C., and M. Ghil, 1988: Cluster analysis of multiple planetary flow regimes. *J. Geophys. Res.*, **93**, 10927-10952

Moise, I., and R. Temam, 2000: Renormalization group method. Application to Navier-Stokes equation. *Discr. Cont. Dyn. Syst.*, **6**, 191-210

Molteni, F., S. Sutera, and N. Tronci, 1988: The EOFs of the geopotential eddies at 500 mb in winter and their probability density distributions. *J. Atmos. Sci.*, **45**, 3063-3080

Molteni, F., S. Tibaldi, and T.N. Palmer, 1990: Regimes in the wintertime circulation over northern extratropics. I: Observational evidence. *Quart. J. Roy. Meteor. Soc.*, **116**, 31-67

Penland, C., and L. Matrosova, 1994: A balance condition for stochastic numerical models with application to the El Nino-Southern Oscillation. *J. Climate*, **7**, 1352-1372

Penland, C., and P.D. Sardeshmukh, 1995: The optimal growth of tropical sea surface temperature anomalies. *J. Climate*, **8**, 1999-2024

Selten, F.M., 1995: An efficient description of the dynamics of barotropic flow. *J. Atmos. Sci.*, **52**, 915-936

Selten, F.M., 1997a: A statistical closure of a low-order barotropic model. *J. Atmos. Sci.*, **54**, 1085-1093

Selten, F.M., 1997b: Baroclinic empirical orthogonal functions as basis functions in an atmospheric model. *J. Atmos. Sci.*, **54**, 2099-2114

Toth, Z., 1995: Degrees of freedom in northern hemisphere circulation data. *Tellus*, **47 A**, 457-472

Van den Dool, H.M., and R.M. Chervin, 1986: A comparison of month-to-month persistence of anomalies in a general circulation model and in the earth's atmosphere. *J. Atmos. Sci.*, **43**, 1454-1466

Vautard, R., and B. Legras, 1988: On the source of midlatitude low-frequency variability. Part II: Nonlinear equilibration of weather regimes. *J. Atmos. Sci.*, **45**, 2845-2867

Vautard, 1990: Multiple weather regimes over the North Atlantic: Analysis of precursors and successors. *Mon. Wea. Rev.*, **118**, 2056-2081

Voss, R., R. Saussen, and U. Cubasch, 1998: Periodically synchronously coupled integrations with the atmosphere-ocean general circulation model ECHAM3/LSG. *Clim. Dyn.*, **14**, 249-266

Wang, X., and S.S. Shen, 1999: Estimation of spatial degrees of freedom of a climate field. *J. Climate*, **12**, 1280-1291

Whitaker, J.S., and P.D. Sardeshmukh, 1998: A linear theory of extratropical synoptic eddy statistics. *J. Atmos. Sci.*, **55**, 237-258

Zhang, Y., and I.M. Held, 1999: A linear stochastic model of a GCM's midlatitude storm tracks. *J. Atmos. Sci.*, **56**, 3416-3435

**Table 1:** For the three cluster centroids in the January data of the 30-EOF semi-empirical model, the steady states of this model and various reduced low-frequency models nearest to each centroid, as well as the total number of steady states $N_f$ found in each model. In the first column f$n$d$\tilde{N}$ denotes the $\tilde{N}$-dimensional model for $n$-day-low-pass filtered January data of the unfiltered model (which is denoted by f0d30). The number of years used in the analysis is also indicated. For each model the upper row contains the relative squared distance $\epsilon_i$ between centroid $i$ and the closest steady state (normalized by the the squared distance of the centroid to the January mean), irrespectively whether the latter is also closest to another centroid. The lower row indicates the distance to the 'closest' steady state so that in the case of a steady state being closest to several centroids the steady-state-centroid pair with the smallest relative distance has been picked, and for the remaining centroids a search among the remaining steady states has been done. Numbers in brackets denote the index of the steady state (arbitrarily ordered).

| model | $N_f$ | $\epsilon_1$ | $\epsilon_2$ | $\epsilon_3$ |
|---|---|---|---|---|
| f30d30 | | 1.94 (1) | 9.81 ( 1) | 6.17 ( 1) |
| (24000a) | 14 | 1.94 (1) | 18.11 ( 4) | 6.19 ( 2) |
| f30d5 | | 1.98 (1) | 8.53 ( 1) | 1.48 ( 1) |
| (6000a) | 5 | 2.23 (4) | 11.21 ( 2) | 1.48 ( 1) |
| f30d3 | | 0.94 (1) | 2.28 ( 2) | 1.71 ( 2) |
| (3000a) | 3 | 0.94 (1) | 548.54 ( 3) | 1.71 ( 2) |
| f5d30 | | 5.50 (2) | 9.89 ( 2) | 3.86 (18) |
| (6000a) | 46 | 5.50 (2) | 13.98 (25) | 3.86 (18) |
| f5d5 | | 2.83 (1) | 3.05 ( 1) | 1.43 ( 3) |
| (6000a) | 5 | 2.83 (1) | 12.90 ( 2) | 1.43 ( 3) |
| f5d3 | | 5.39 (1) | 10.96 ( 1) | 1.02 ( 1) |
| (3000a) | 3 | 6.41 (2) | 2493.90 ( 3) | 1.02 ( 1) |
| f0d30 | | 3.03 (3) | 13.38 ( 4) | 7.27 ( 6) |
| (1500a) | 22 | 3.03 (3) | 13.38 ( 4) | 7.27 ( 6) |

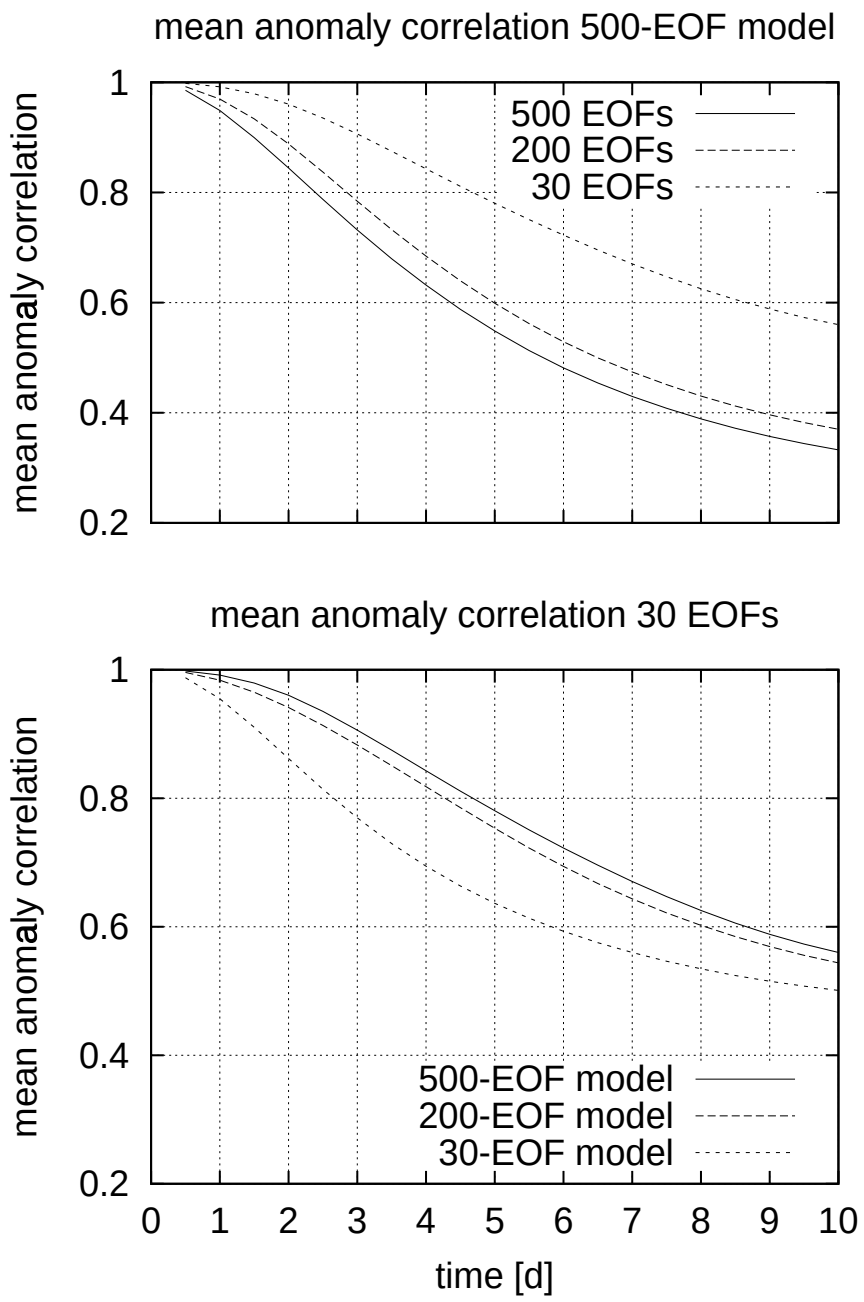


**Figure 1**: Mean anomaly correlations between GCM trajectories and those obtained by integration of three semi-empirical models. Upper Panel: Correlation for the 500-EOF model, calculated in the subspace of the leading 500, 200, and 30 EOFs. Lower Panel: Correlation in the subspace of the leading 30 EOFs, obtained by integrating the 500-, 200-, or 30-EOF model.

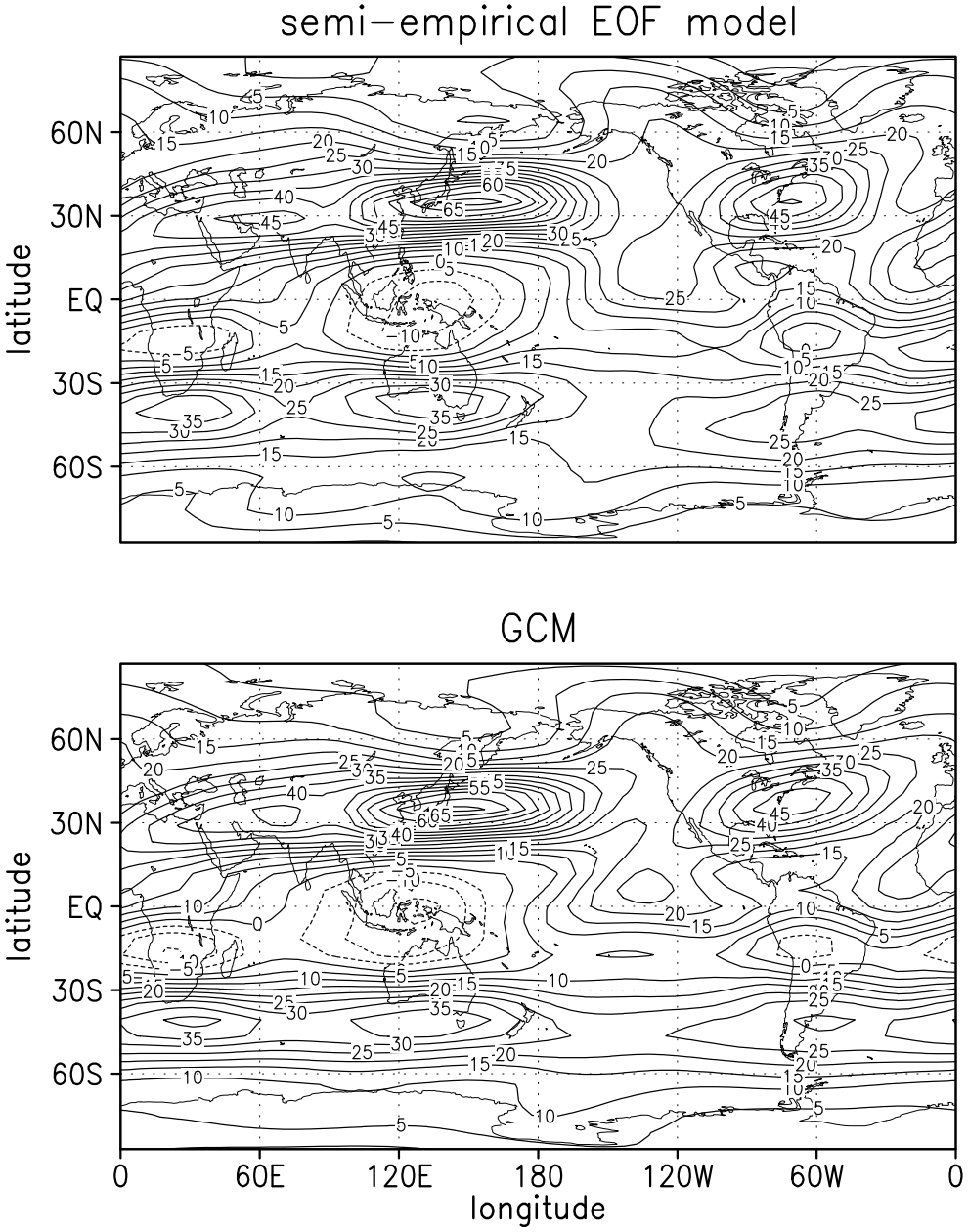


**Figure 2**: The January mean zonal wind at $\sigma = 0.167$, as simulated by the GCM, and by the semi-empirical 500-EOF model. Units are m/s.

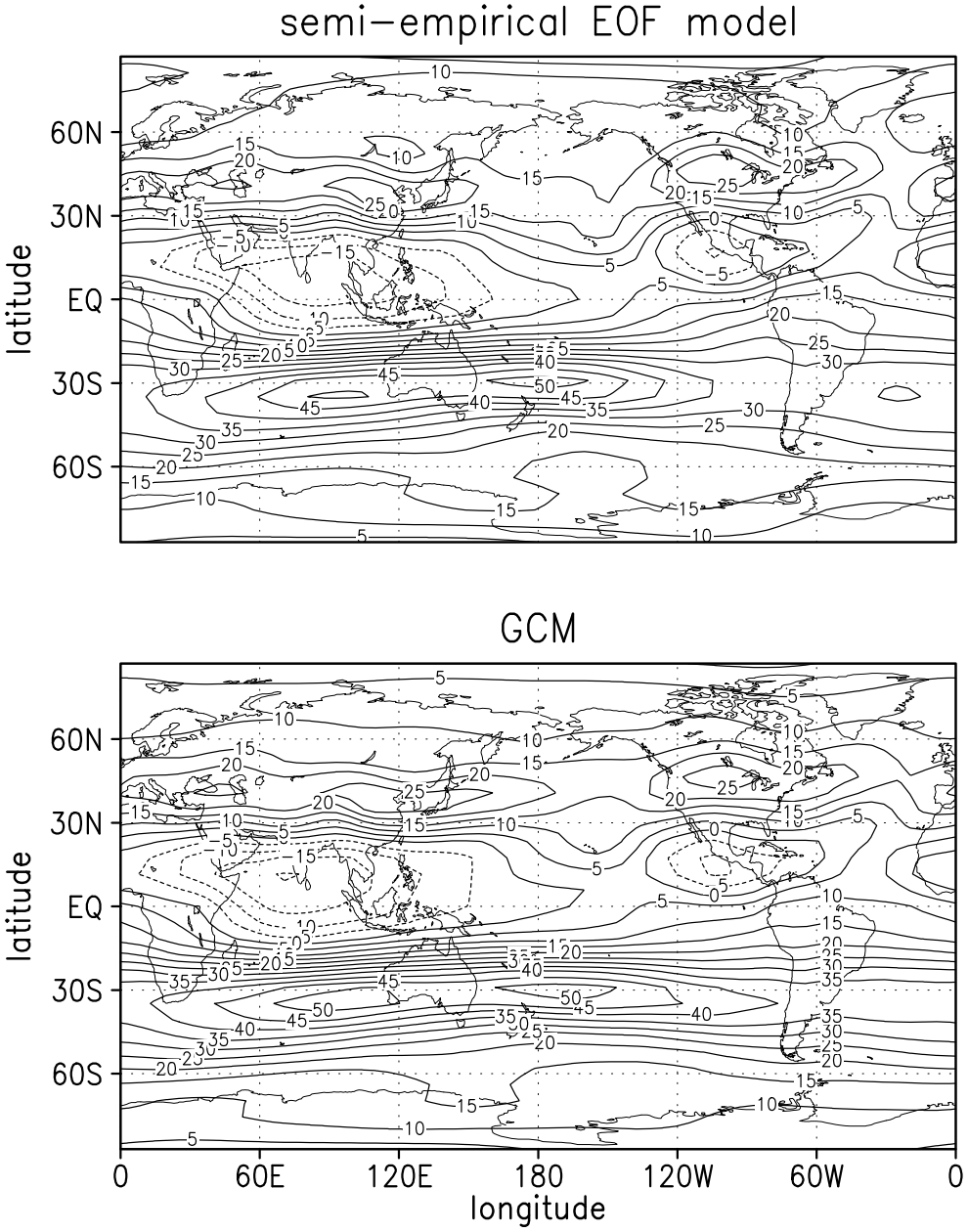


**Figure 3**: As Fig. 2, but for July.

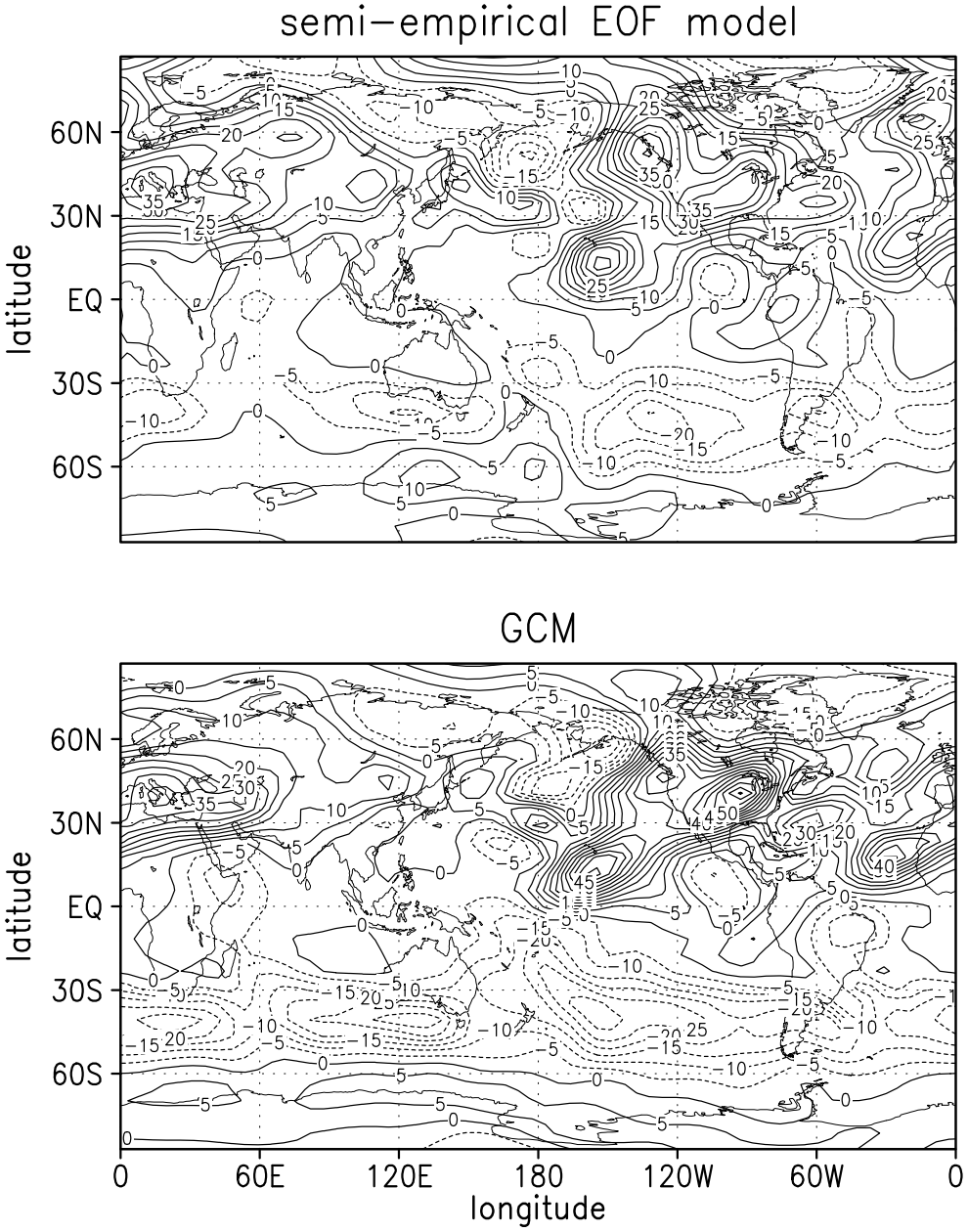


**Figure 4**: The January mean meridional momentum transport by the transients (at $\sigma = 0.167$), projected onto the leading 500 EOFs, as simulated by the GCM, and by the semi-empirical 500-EOF model. Units are $m^2/s^2$.

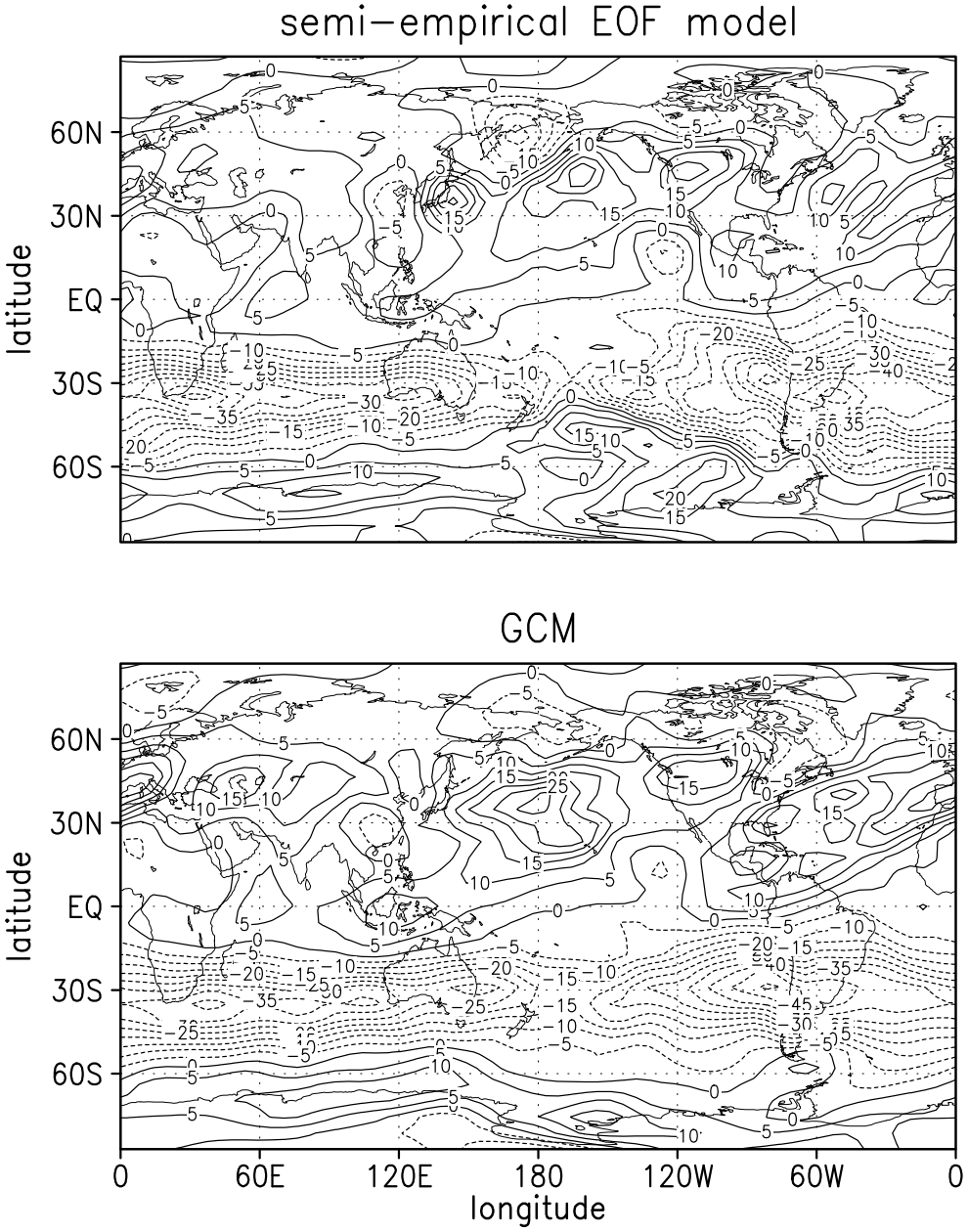


**Figure 5**: As Fig. 4, but for July.

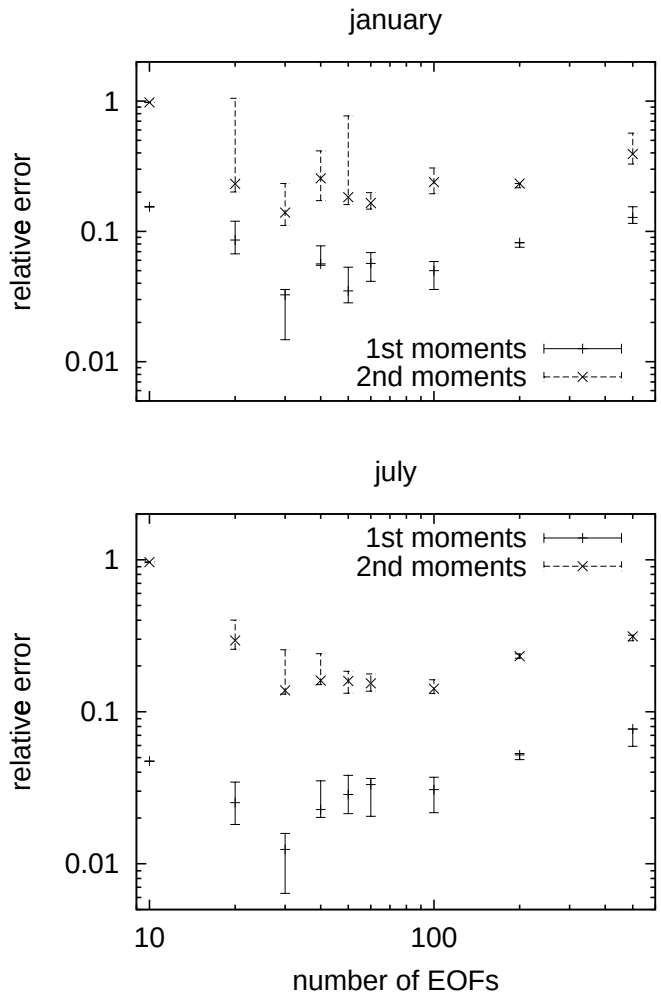


**Figure 6**: The relative errors in the simulation of the first and second moments of the GCM by reduced models with different resolution. The errors are computed within the subspace resolved by each model. Shown are the results for January and July. The error bars (around the errors of the model optimally tuned with respect to the overall climate error) have been obtained by picking the smallest and largest monthly moment error among all cases examined in the optimization of the additional model dissipation (cf. AO for details) where the mean relative deviation between the optimal dissipation parameter set and the actual parameter set was less than 1%.

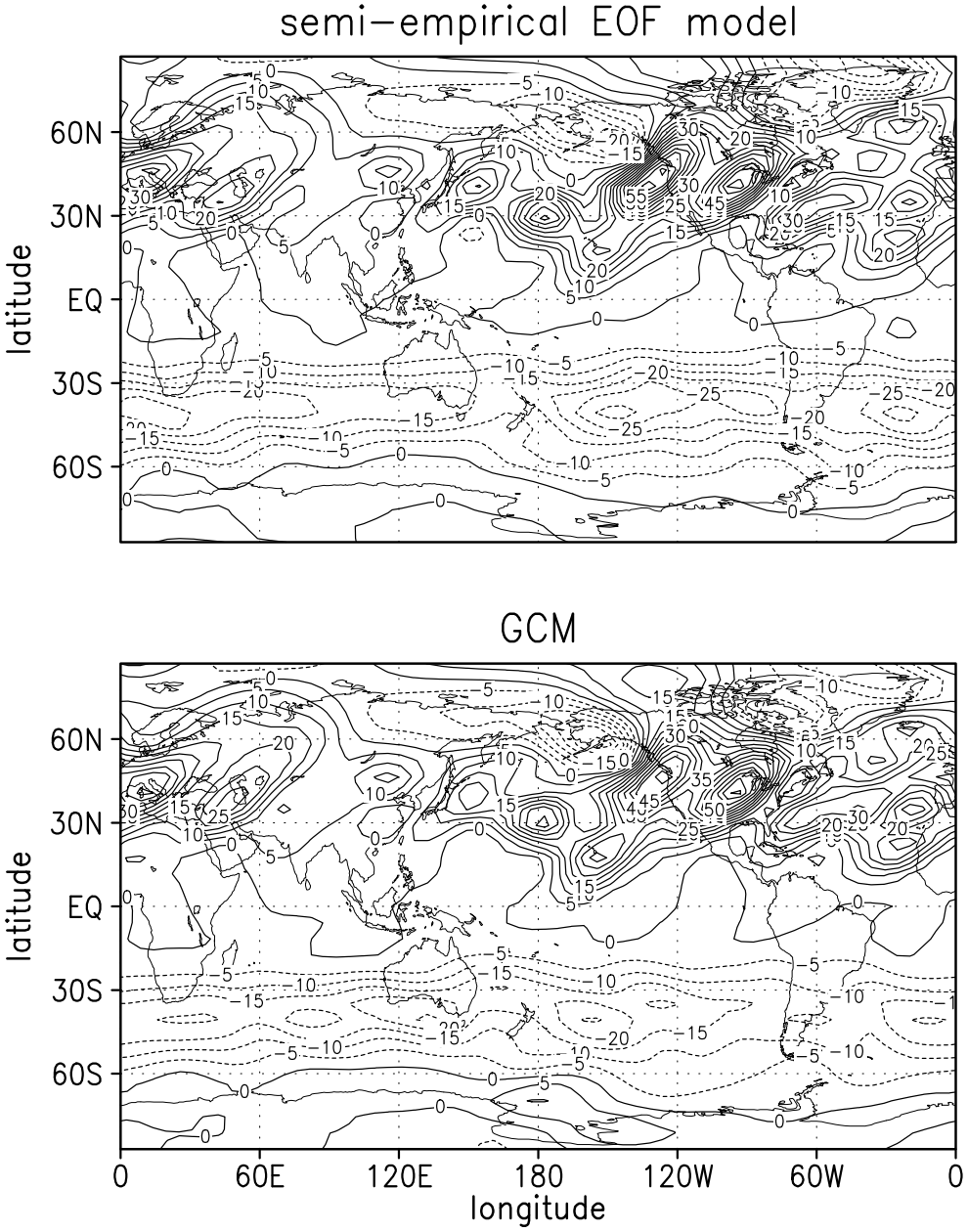


**Figure 7**: As Fig. 4, but for the simulation of the January mean meridional momentum transport by the semi-empirical 30-EOF model.

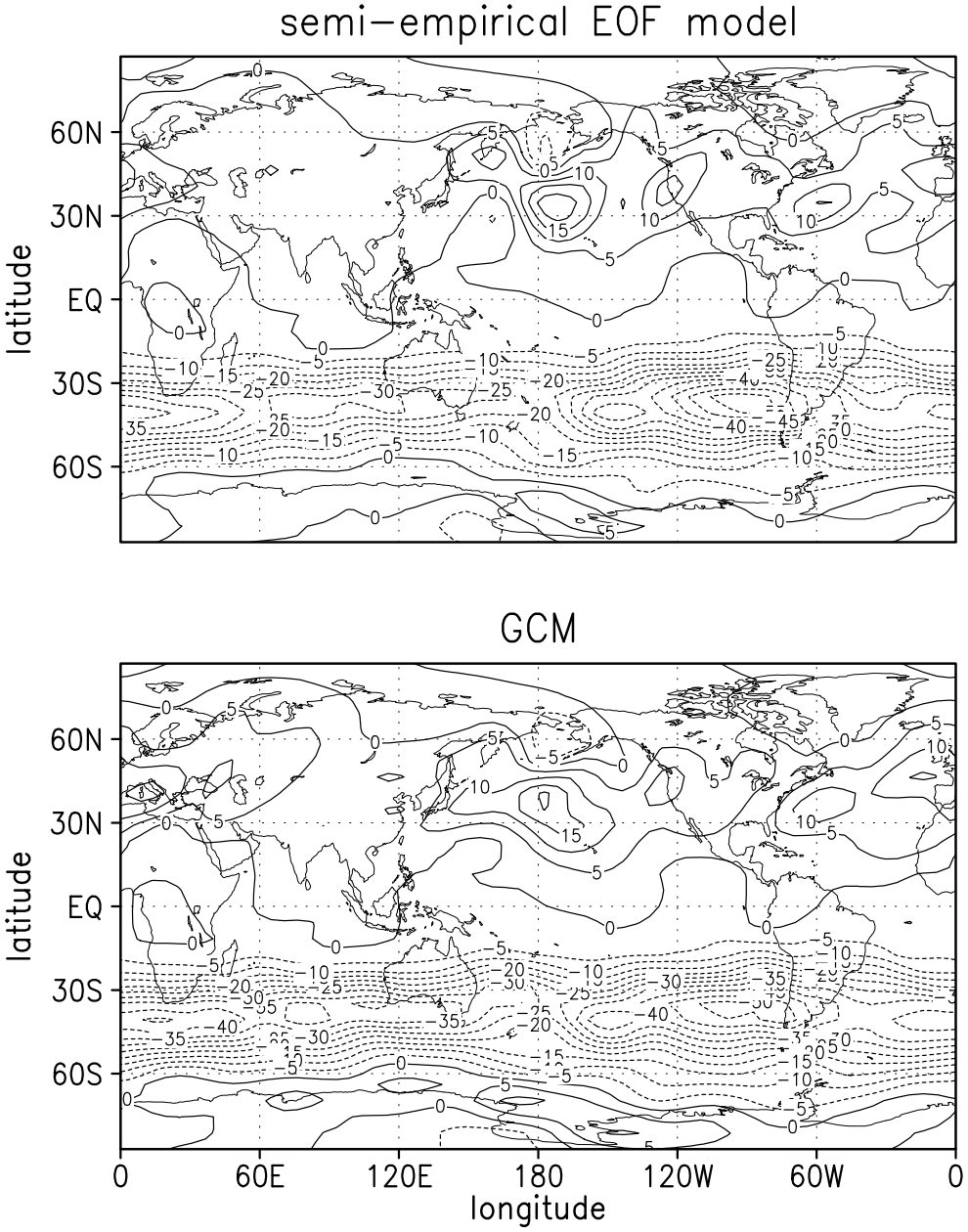


**Figure 8**: As Fig. 7, but for July.

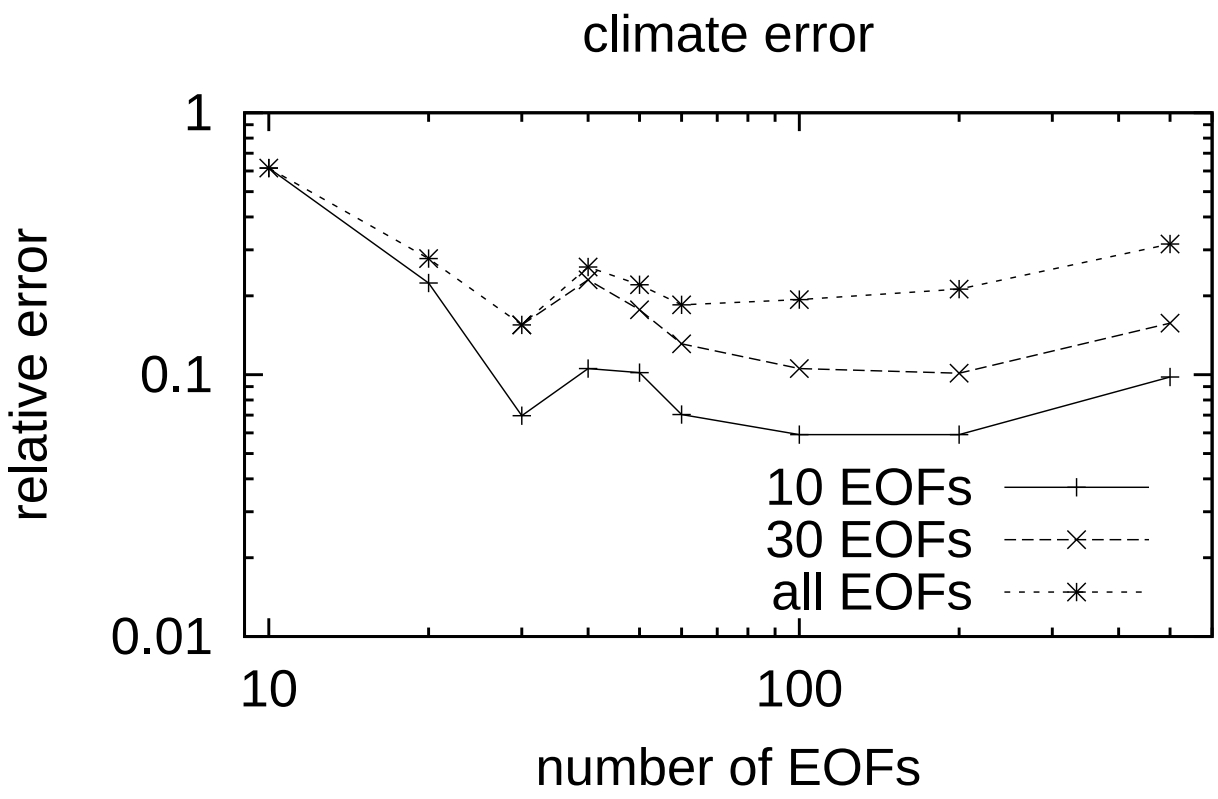


**Figure 9**: The climate error of several optimally tuned reduced models, characterizing their performance in simulating the seasonally-dependent first and second moments. The calculation has been done in the subspace of the leading 10 EOFs, the leading 30 EOFs, and all EOFs the respective model is based on.

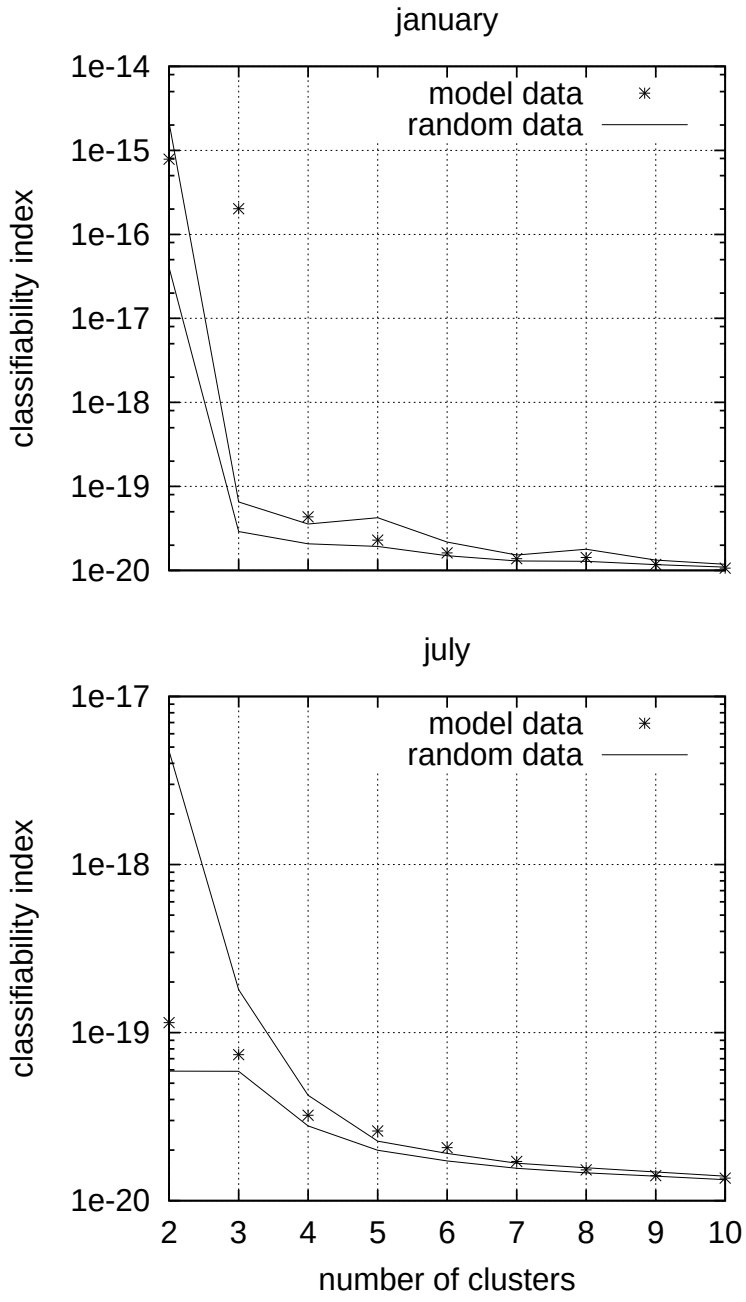


**Figure 10**: Classifiability of the GCM data, low-passed filtered by averaging over 5 days, depending on the number of clusters determined in a cluster analysis. The analyzed subspace consists of the coefficients belonging to the leading 30 GCM-EOFs. In the upper panel 1500 January months have been analyzed, in the lower panel the same number of July months.

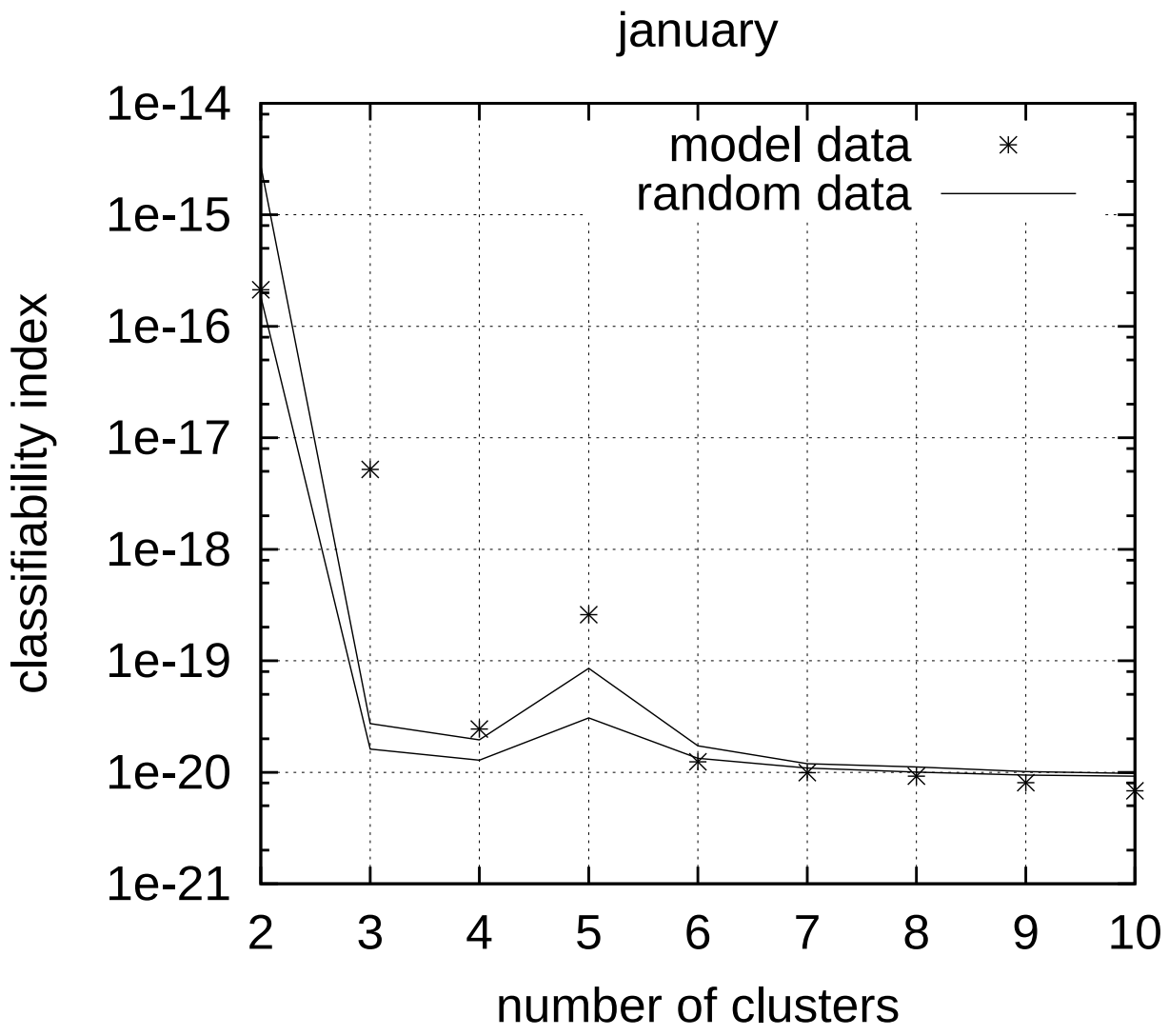


**Figure 11**: As the upper panel of Fig. 10, but for the data from the semi-empirical 30-EOF model.

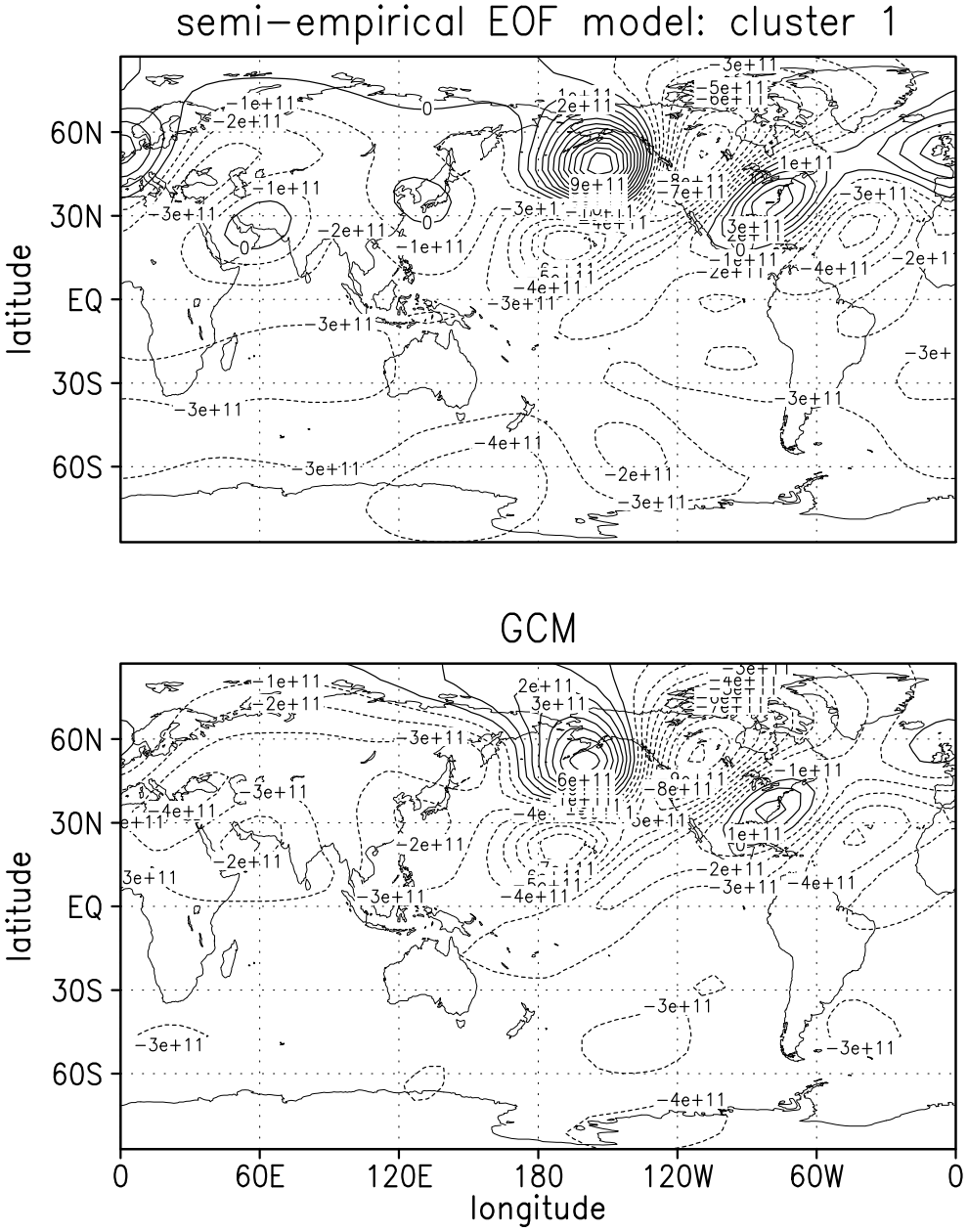


**Figure 12**: Barotropic streamfunction anomaly with respect to the January mean state in the first cluster centroid determined in a three-cluster partition of the time-filtered January data set from the semi-empirical 30-EOF model (upper panel), and from the GCM (lower panel). Units are Pa $m^2/s$. The percentage of GCM states in the cluster is 30%, the corresponding number for the reduced model 27%.

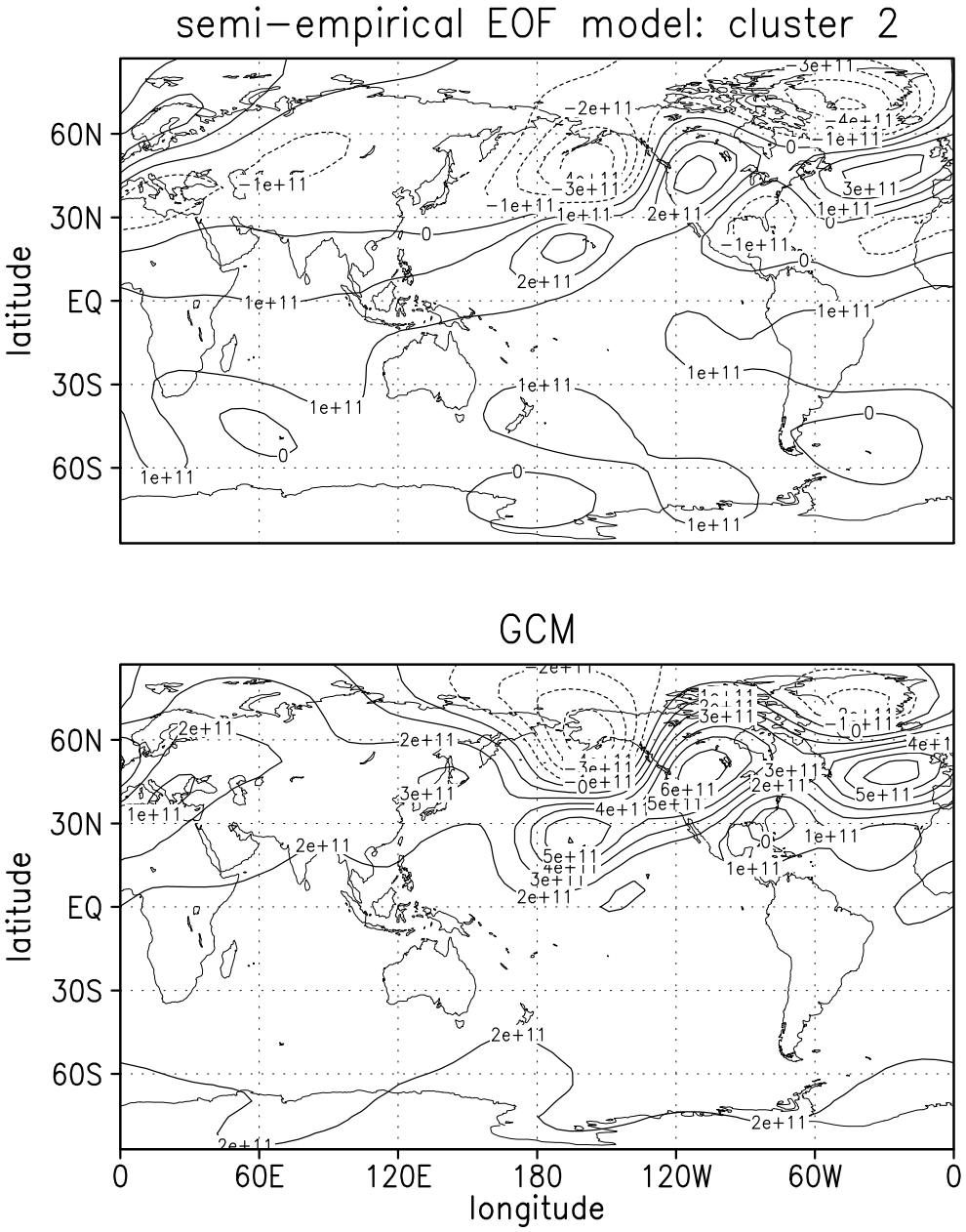


**Figure 13**: As Fig. 12, but for cluster 2, with the percentage of GCM-states in the cluster being 40%, the one of reduced-model states in the cluster 38%.

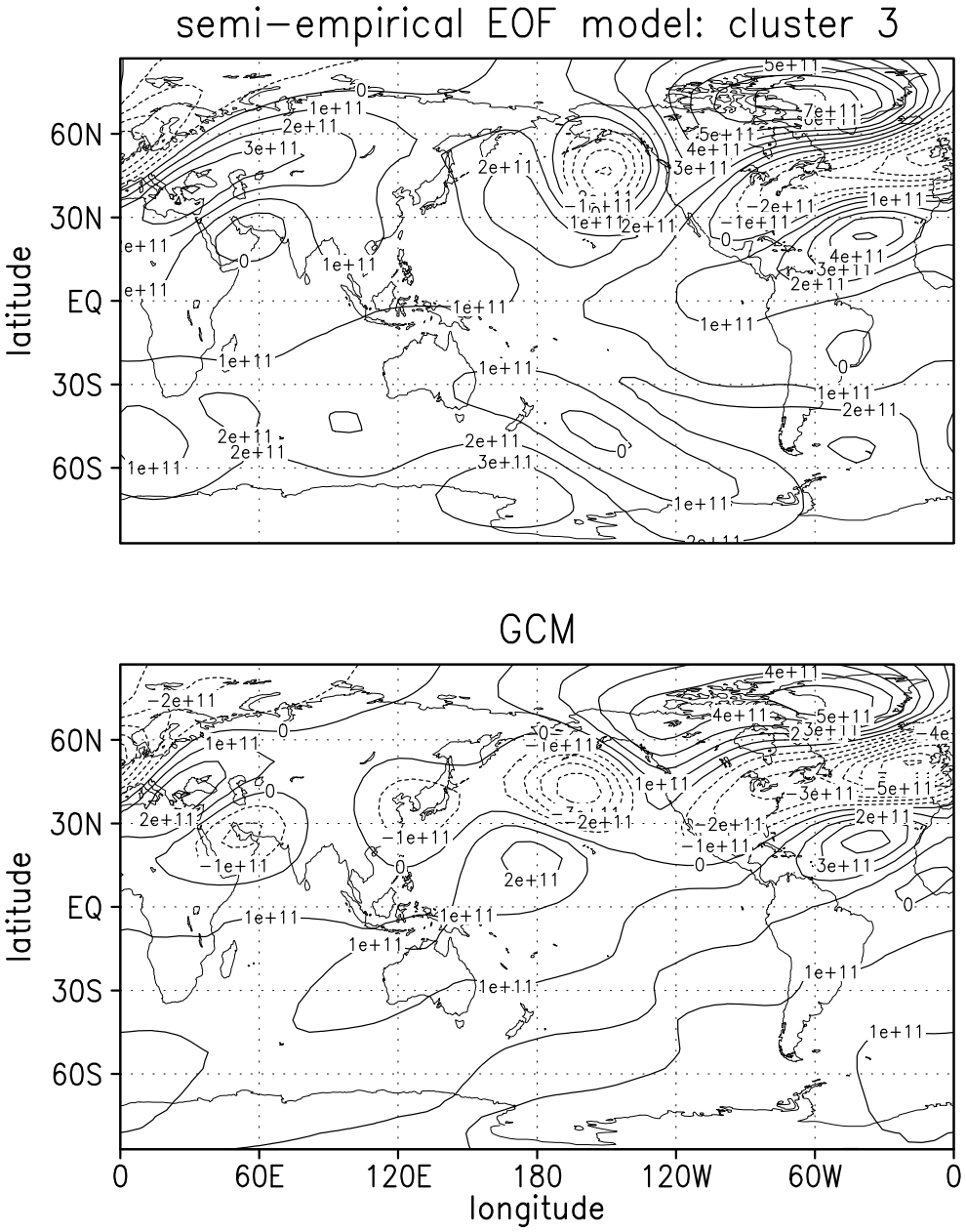


**Figure 14**: As Fig. 12, but for cluster 3. 30% of all GCM states are in this cluster, and 35% of all analyzed states from the 30-EOF model.

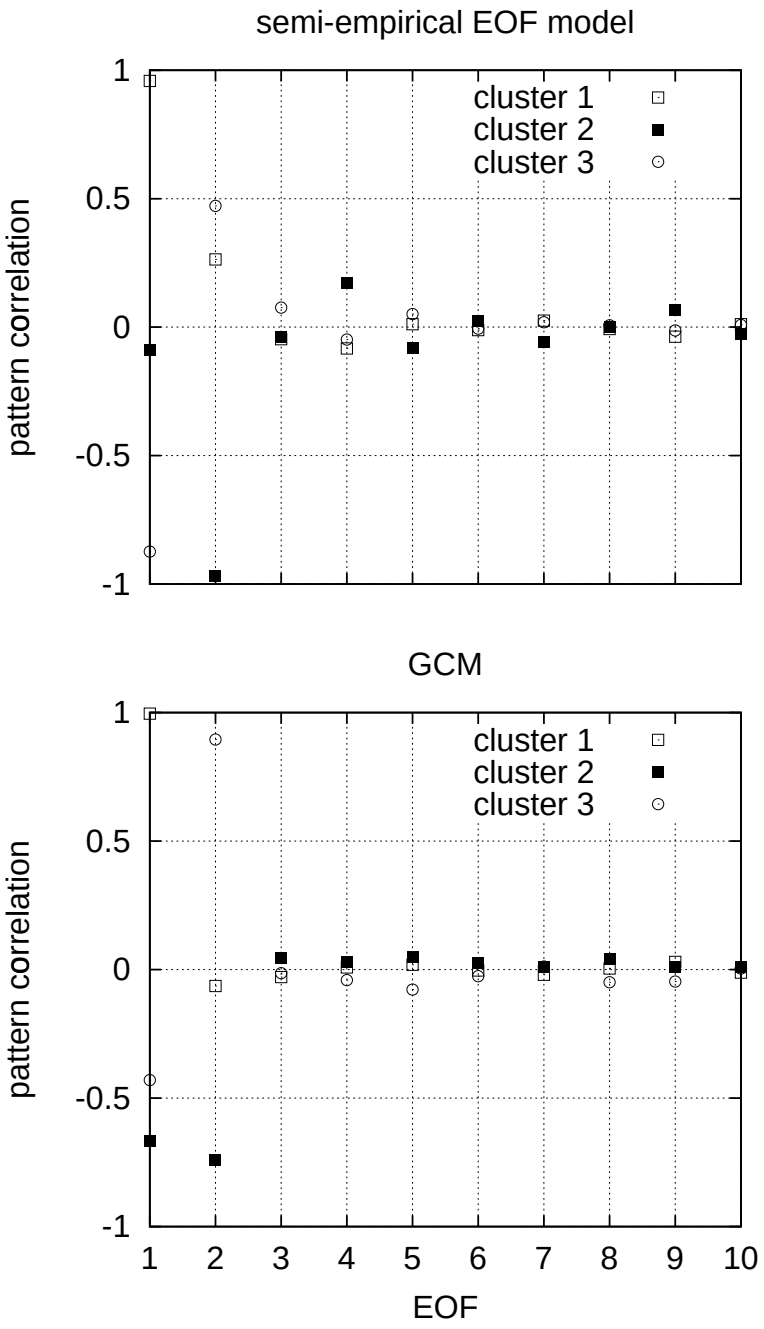


**Figure 15**: For January, the pattern correlations between the anomalies of the three significant clusters with respect to the monthly-mean state and the ten leading low-frequency EOFs (5-day low-pass filter), in the 30-EOF model (top) and the GCM (bottom).

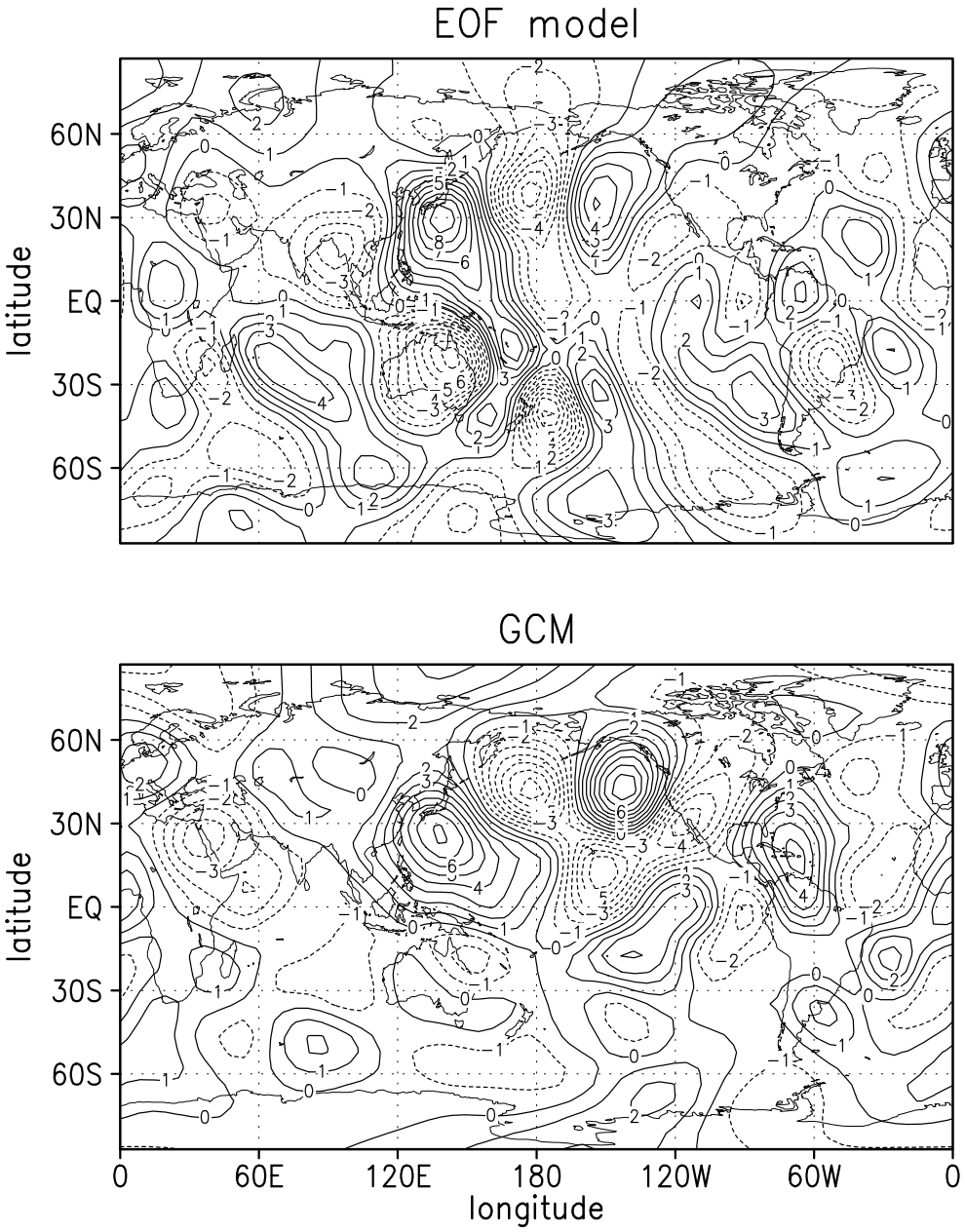


**Figure 16**: Response in the meridional wind in the layer at $\sigma = 0.167$ to anomalous heating over the equator at 150°E in the semi-empirical EOF model with 200 tropical $\tau$-EOFs and 500 EOFs for global winds, barotropic streamfunction and extratropical $\tau$ (top), and in the GCM (bottom). Both models have been integrated under perpetual-January conditions. Units are m/s.

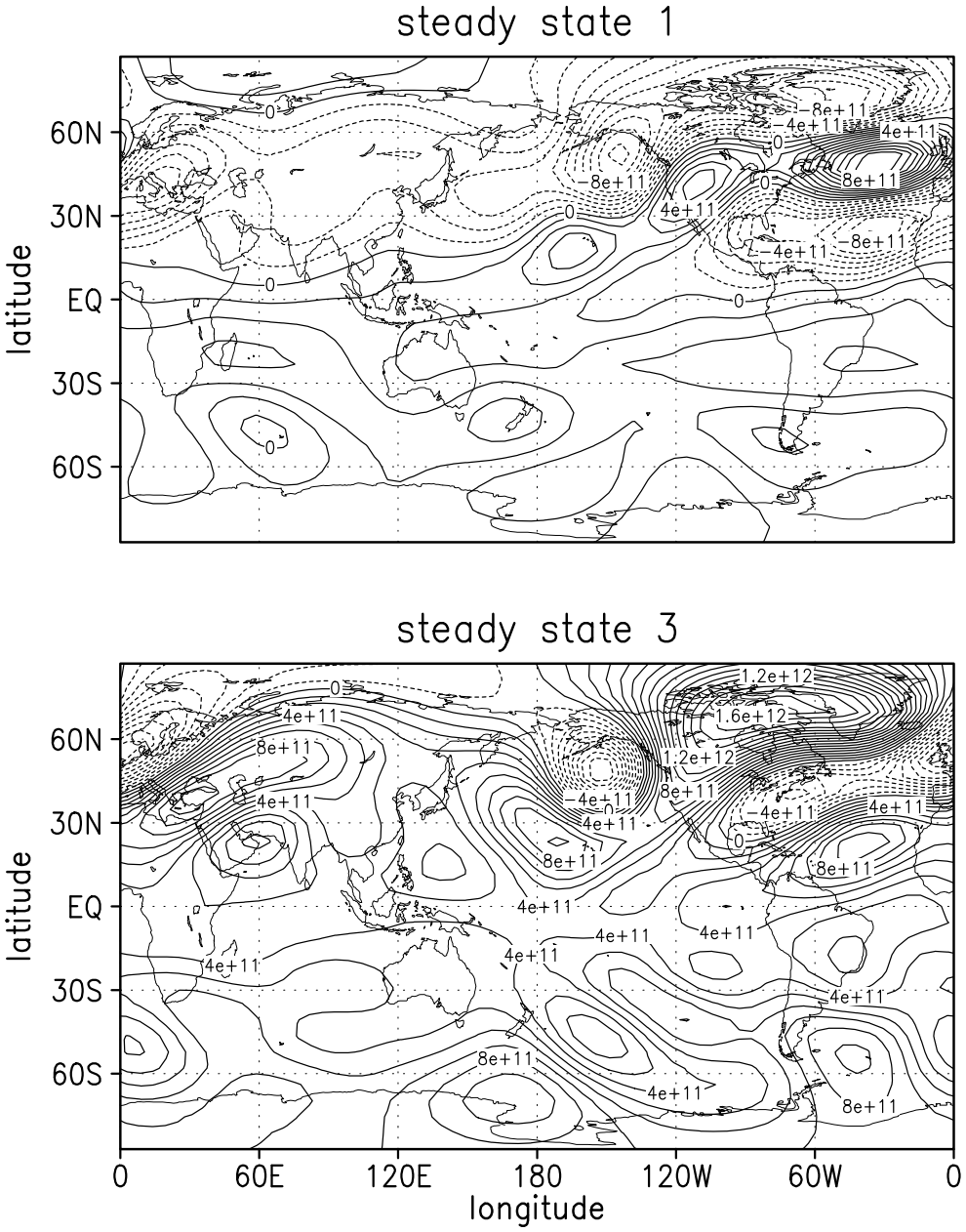


**Figure 17**: Barotropic streamfunction anomalies with respect to the January mean of the two steady states of the 5-dimensional 5-day-low-pass low-frequency model closest to cluster centroids 1 and 3 as shown in figures 12 and 14. Units and contours are the same as there.